General Disclaimer

One or more of the Following Statements may affect this Document

- This document has been reproduced from the best copy furnished by the organizational source. It is being released in the interest of making available as much information as possible.

- This document may contain data, which exceeds the sheet parameters. It was furnished in this condition by the organizational source and is the best copy available.

- This document may contain tone-on-tone or color graphs, charts and/or pictures, which have been reproduced in black and white.

- This document is paginated as submitted by the original source.

- Portions of this document are not fully legible due to the historical nature of some of the material. However, it is the best reproduction available from the original submission.

RSI-SDSU-75-09

SOIL MOISTURE AND EVAPOTRANSPIRATION PREDICTIONS USING SKYLAB DATA

Remote Sensing Institute
South Dakota State University
Brookings, South Dakota 57006

TECHNICAL REPORT STANDARD TITLE PAGE

1. Report No.	2. Government Accession No.	3. Recipient's Catalog No.

4. Title and Subtitle	5. Report Date
Soil Moisture and Evapotranspiration Predictions using SKYLAB Data	6. Performing Organization Code

7. Author(s)	8. Performing Organization Report No.
Moore, D.G., M.L. Horton, M.J. Russell, and V.I. Myers	SDSU-RSI-75-09

9. Performing Organization Name and Address	10. Work Unit No.
Remote Sensing Institute South Dakota State University Brookings, South Dakota 57006	11. Contract or Grant No. NAS 9-13337
	13. Type of Report and Period Covered Final Report 3/1/73 - 9/30/75
12. Sponsoring Agency Name and Address National Aeronautics and Space Administration Lyndon B. Johnson Space Center Houston, Texas 77058	14. Sponsoring Agency Code

15. Supplementary Notes

Original photography may be purchased from:
EROS Data Center
10th and Dakota Avenue
Sioux Falls, SD 57198

ORIGINAL CONTAINS COLOR ILLUSTRATIONS

16. Abstract Multispectral reflectance and emittance data from the SKYLAB workshop were evaluated for prediction of evapotranspiration and soil moisture for an irrigated region of Southern Texas. Regression equations were developed using the S192 data for prediction of the 0→30 cm gravimetric soil moisture for fallow surfaces and for surfaces of variable crop cover which had multiple correlation coefficients as large as 0.95 and 0.74, respectively. The use of thermal emittance measurements for assessing evapotranspiration was developed. Evapotranspiration maps were produced using the Jensen-Haise prediction model and emittance data from SKYLAB. Rationale for using the remotely sensed data for estimating crop coefficients was discussed. A data reduction method required for utilizing field spectral measurements in an operational irrigation scheduling program was developed and illustrated. Enhancement methods for thematic mapping using digital scanner data were developed based upon statistical procedures and were illustrated using S192 data. Thematic maps of irrigated lands were prepared. The recommended spectral regions for scanners on future satellites should include at least the 10.2→12.5 μm, 1.55→1.75 μm, 0.56→0.61 μm, and 0.98→1.08 μm spectral regions. Operational uses of emittance data were discussed and procedures were outlined for surveying areas of high soil moisture, scheduling irrigation, and providing inputs to water budgets of regions.

17. Key Words Suggested by Author	18. Distribution Statement
thermal emittance soil moisture evapotranspiration irrigation scheduling soil thermal properties	

19. Security Classif. (of this report)	20. Security Classif. (of this page)	21. No. of Pages	22. Price

Organization:	Remote Sensing Institute South Dakota State University Brookings, South Dakota 57006
Report Title:	Soil Moisture and Evapotranspiration Predictions using SKYLAB Data
Report Type:	Final Report
EREP Investigation Number:	S452
NASA Contract Number:	NAS 9-13337
Authors:	D.G. Moore, Research Soil Scientist M.L. Horton, Prof. of Plant Science in Water Resources M.J. Russell, Staff Specialist V.I. Myers, Director
Principal Investigator:	V.I. Myers
Date Submitted:	October 1975
NASA Technical Monitor:	Ryborn R. Kirby Operations Room Code TF6 Johnson Space Center Houston, Texas 77058

Additional reports or papers submitted under Contract NAS 9-13337:

Moore, D.G., M.L. Horton, and M.J. Russell. 1974. Preliminary Evaluation of S-192 SKYLAB Data for Assessing Energy Exchange and Land Use in Irrigated Agriculture. Advanced Report of Significant Results. SDSU-RSI-74-18. 58 pp.

Russell, M.J., D.G. Moore, G.D. Nelson, and V.I. Myers. 1974. Boundary-Detection Algorithm for Locating Edges in Digital Imagery. Advanced Report of Significant Results. SDSU-RSI-74-10. 28 pp.

Moore, D.G., M.L. Horton, M.J. Russell, and V.I. Myers. 1975. Evaluation of Thermal X/5-Detector SKYLAB S-192 Data for Estimating Evapotranspiration and Thermal Properties of Soils for Irrigation Management. Proceedings of Earth Resources Survey Symposium at Houston, Texas, June 8-13, 1975. In press. SDSU-RSI-J-75-03.

ACKNOWLEDGEMENTS

The authors wish to acknowledge Mr. Clayton Forbes and Mr. Ryborn Kirby, NASA PIMO leaders, for their advice and assistance throughout the effort and especially for help in preparation of this document. Ms. C.A. Reeves and Mr. David Faulkner, Lockheed Scientists, are gratefully acknowledged for preparation of the products from the DAS system at JSC. Innumerable land owners gave permission for use of their lands. The final test site was the Reynolds-Wilson Farm of Carrizo Springs, Texas. Various Institute staff were invaluable in collecting, reducing, and analyzing the ground and aerial data and in preparing of the final manuscript. Mr. Dennis Ryland in ground data collection and analysis; Mr. Michael Wehde, Ms. Mary DeVries, and Mr. Darrell Hause in statistical reduction of the data; Mr. Alvin Rusche and Mr. William Rippert in aerial data collection; Mr. Jack Smith and Ms. Mary Buckmiller for photographic processing; Mr. Robert Best, Ms. Janet Hamiel, Ms. Shari Sparrow, Ms. Cindy O'Connor, and Ms. Geri Bushard for preparation of the final manuscript. Dr. Gerald Nelson was invaluable in assistance for developing the statistical and pattern recognition procedures applied to the digital data. The South Dakota Water Resources Institute cooperative efforts are gratefully acknowledged.

TABLE OF CONTENTS

TABLE OF CONTENTS (continued)

LIST OF FIGURES

LIST OF FIGURES (continued)

LIST OF TABLES

LIST OF TABLES (continued)

INTRODUCTION

The surface of the earth continually absorbs and emits energy. The balance achieved between energy inputs and energy outputs represents the energy budget. Models have been developed to simulate the complex interactions among the energy budget components. Ground-based meteorological point-sample measurements have been used as inputs for verification of model accuracies. These models can be used with data from aircraft and satellites equipped with sensors capable of measuring reflected and emitted energy. The remote sensor offers a synoptic, yet detailed, approach for studying and using concepts from the energy budget for resource monitoring over a variety of landscape variables on a repetitive basis.

The temperature of a fallow soil or vegetated surface is an integral response by that surface to environmental factors such as level of incoming radiation, air temperature and humidity, wind speed, etc. Such surface characteristics as albedo, roughness, wetness, and other physical parameters alter the effect of the environmental factors on the energy budget and heat exchanges and consequently are expressed as temperature variations.

A major source or sink of heat energy in the soil-plant environment is water. Water plays a major role in conduction and convection of heat to and from the soil surface. In addition, phase changes of water by vaporization and fusion absorb and release large quantities of heat. Fallow soil surfaces dissipate a portion of the incoming energy by evaporation. Dissipation of energy by evaporation from plants is termed transpiration. A land surface having a crop canopy dissipates energy by evaporation from both the plant and the soil which is collectively termed evapotranspiration (ET). Soil moisture and evapotranspiration estimates using remote-sensor data could provide a powerful management tool for irrigation scheduling, crop yield predictions, detecting disease and insect infestations, flood forecasting, predicting seed germination, monitoring land-erosion potential, and numerous other applications.

OBJECTIVE

To determine the physical and thermal properties of the surface and subsurface soils and to measure the surface temperature and emitted radiation by use of remotely sensed data.

BACKGROUND

Energy Budget

According to Sellers (1965), approximately 30% of the solar radiation reaching the outer boundary of the earth's atmosphere is reflected and scattered back into space by clouds, aerosols, and other atmospheric constituents. Approximately 17% of the incoming radiation is absorbed by the earth's atmosphere and about 22% reaches the earth's surface as diffuse radiation. Therefore, only about 31% of the radiation entering the outer boundary of the earth's atmosphere reaches the surface as direct solar radiation.

Incoming radiation received at the earth's surface is either absorbed, reflected, or transmitted. Absorbed short-wave radiation may be emitted at a later time at a longer wavelength; therefore, solar radiation may be absorbed, stored in the crop canopy or soil, and emitted later as thermal radiation. A portion of the absorbed radiation can be used to evaporate water. The heat of vaporization used in the evaporation process may subsequently be transferred from the surface as a vapor flux.

That portion of the radiation in the energy budget which is the difference between total incoming and total outgoing radiation is termed net radiation. Mathematically, net radiation (R_n) can be expressed as

$$R_n = (R_S + R_s + R_T) - [\alpha (R_S + R_s) + R_{TO}] \qquad [1]$$

where R_S is direct incoming shortwave radiation, R_s is diffuse incoming shortwave radiation, R_T is incoming longwave radiation, R_{TO} is outgoing longwave radiation, and α is the albedo of the surface. Since albedo directly affects the net radiation, remote monitoring of albedo provides information about the energy absorption characteristics of a surface. The absorbed energy is potentially available for the evaporation of water, for heat storage, etc. In addition, reflectance within specific wavebands may serve as an indicator of certain physical and biological

properties. For example, surface water has a unique spectral signature in the longer reflective-infrared wavelengths which can be used to thematically map the occurrence of water. The evaporation rate of free water surfaces is limited only by energy budget conditions and not by the transport of water to the evaporating surface.

The net radiation may be utilized at the earth's surface as

$$R_n + S + A + LE + P + M = 0 \qquad [2]$$

where S is soil heat flux, A is sensible heat flux in the air, LE is heat flux due to evapotranspiration, P is the energy used in photosynthesis, and M represents a miscellaneous energy term. For some applications, equation [2] is used as an energy balance equation where only surface elements are considered and storage plus divergence terms are neglected. However, energy may be transferred into or away from a volume element of the surface by advection of sensible and latent heat which may be expressed as

$$\text{Advection} = \int_o^\zeta C_p \nabla(\rho\mu T)\, dz + \int_o^\zeta \frac{L\varepsilon}{R} \nabla\left(\frac{\mu e}{T}\right) dz \qquad [3]$$

where z is distance along the path, ζ is a defined upper boundary, C_p is the specific heat of air, ∇ is $\frac{\partial}{\partial z} + \frac{\partial}{\partial y}$, ρ is air density, μ is wind speed, T is temperature, L is latent heat of vaporization, ε is water vapor flux, R is the universal gas constant, and e is the vapor pressure of the air.

Energy can be stored in a volume element of the earth's surface in the form of heat content of the crop, sensible heat in the air, and latent heat of the air. These storage terms may be represented as

$$\text{Storage} = \int_o^\zeta Q\rho c \left(\frac{\partial T}{\partial t}\right) dz + \int_o^\zeta C_p \rho \left(\frac{\partial T}{\partial t}\right) dz + \int_o^\zeta \frac{L\varepsilon}{RT} \left(\frac{\partial e}{\partial t}\right) dz \qquad [4]$$

where Q is the heat capacity of the crop, ρc is the crop density, ε is the ratio of molecular weight of water to air, t is time, and the other terms are as previously defined.

Utilizing the energy budget terms developed for an element $\delta x \delta y \delta z$ of the earth's surface when a crop canopy or other rough surface is present, an energy budget equation can be formulated. The complete

energy balance equation is

$$R_n + S + A + LE + P + M + \int_0^\zeta C_p \nabla(\rho\mu T)\, dz + \int_0^\zeta \frac{L\varepsilon}{R} \nabla(\frac{\mu e}{T})\, dz + \int_0^\zeta Q\rho c\, (\frac{\partial T}{\partial t})\, dz + \int_0^\zeta C_p\rho\, (\frac{\partial T}{\partial t})\, dz + \int_0^\zeta \frac{L\varepsilon}{RT}\, (\frac{\partial e}{\partial t})\, dz = 0 \qquad [5]$$

where all terms have been previously defined.

The relative magnitude of the storage terms is negligible during most of the day. However, the error introduced by neglecting the storage terms can be appreciable for a short period near sunrise when R_n, A, and E are small and $\frac{\partial T}{\partial t}$ is large (Tanner, 1960). Tanner found that at night (midnight to 0600 hours) the storage terms of an alfalfa brome canopy were about 6% of the soil heat flux and about 2% of the net radiation. The horizontal divergence terms may be large if the area is small and permits air passage through the crop (Tanner, 1960). Divergence may also be high where an irrigated field is surrounded by a dry area. Divergence is normally negligible well inside large fields where border or other external influences are small.

The flux direction of the energy balance components are dependent on time of day and climatic conditions. During the day, radiation from the sun is absorbed by the soil and the crop. Thus, the soil and crop surfaces may become warmer than the air so that sensible heat flux is away from the crop volume. During the day under stable conditions, the soil surface is warmer than the soil at greater depths so that the soil heat flux is downward away from the crop volume. At night, soil and crop surfaces lose heat through the emission of longwave radiation which is nearly always greater than atmospheric counter-radiation; therefore, soil heat flux is toward the crop volume to counteract the radiation loss. At night, the air is normally cooler than the crop and soil surfaces resulting in sensible heat flux away from the crop volume.

If water is available for evaporation, the latent heat flux is away from the crop volume during the day. At night, latent heat flux may be away or toward the crop volume depending on the respective temperatures of the air, crop, and soil surfaces. In regions with dry climates, latent heat flux will normally continue to be away from the crop volume both day and night and dew formation will not occur.

However, when the crop or soil temperature is less than the dew point temperature, the latent heat flux will be toward the crop canopy. Horizontal divergence terms will normally be greater during the day than during the night due to higher wind speed.

The energy balance components which have been discussed are for micro-climatic regimes such as agricultural fields or portions of fields. Over large macro-climatic land areas, horizontal divergence terms may be neglected. For long-term periods, storage terms may be neglected because energy stored at one time is ultimately released at another time. For example, heat stored in the soil and crop during the day is released at night.

Evapotranspiration

Equation [5] may be used to describe the energy balance of a vegetated land surface. If advection, storage, and miscellaneous energy terms are neglected, equation [5] becomes

$$Rn + S + LE + A = 0 \qquad [6]$$

for a crop canopy. The energy balance equation can be solved to determine evapotranspiration utilizing the Bowen ratio (Bowen, 1926). The Bowen ratio (B) is the ratio of sensible heat (A) transport to latent heat (LE) transport. Using the Bowen ratio, equation [6] may be written as

$$LE = -(Rn + S) / 1 + B \qquad [7]$$

where LE is the evaporative flux or evapotranspiration rate for a cropped surface and B is the Bowen ratio or A/LE. Additional predictive models using energy budget, mass transfer, or combination equations have been developed to estimate the evaporative flux. Bartholic, Namken, and Wiegand (1970), McGuinness and Bordne (1972), Stone and Horton (1974), and Rosenberg, Hart, and Brown (1968) have reviewed and evaluated several of the models. The prediction normally estimates the potential ET in contrast to the actual ET. Morton (1969) has stated that with adequate moisture supplied to the evaporating soil and vegetated surfaces, the actual ET is accurately estimated from the potential ET on a regional basis. However, this relationship is erroneous for surfaces which are not well watered. Remote sensing may provide a method of detecting

and mapping these well-watered and dry surfaces for improving the application of existing models.

An example ET equation is the one derived by Wiegand and Bartholic (1970) which uses surface temperature in estimating potential evaporation from a wet surface. The crop canopy is assumed to be a wet surface at the saturation vapor pressure; therefore, the canopy vapor pressure is a function of the prevailing canopy temperature. Evapotranspiration as expressed by their equation is

$$E_p = -(Rn+S) \; / \; \{1 + G \; [(T_a-T_o)/e_a' - e_o')]\} \qquad [8]$$

where E_p is the potential evapotranspiration, T_a is air temperature at height 'a' above the surface, T_o is surface temperature, e_a' is the saturated water vapor pressure at height 'a', and e_o' is the saturated vapor pressure of the evaporating surface at temperature T_o. Equations employing a surface temperature parameter can be applied for evapotranspiration predictions using remotely sensed emittance estimates of temperature. However, when a surface is comparatively dry or the soil moisture is limiting to the crop canopy, the air in the canopy is not at saturation so the vapor pressure can not be predicted using the remote temperature measurements.

The Jensen-Haise model for potential ET prediction (based on temperature and radiation) was developed and evaluated over large areas of the world (Jensen and Haise, 1963). The model is extensively used for irrigation scheduling and has input parameters as

$$ET_p = (0.025\ T + 0.08)\ R_s \qquad [9]$$

where ET_p = potential ET in mm min^{-1}

T = air temperature in degrees C

R_s = equivalent depth of evaporation of incoming solar radiation in mm/min^{-1}.

Although air temperature is used, the temperature of the evaporating surface should be an improved parameter for estimating actual ET. The same is probably true for R_s.

The Jensen-Haise ET_p is frequently modified for actual evapotranspiration using a crop coefficient, Kc. The crop coefficient varies

from near zero to slightly more than 1.0, depending upon the growth stage and type of crop. During the period of maximum vegetative cover, Kc will be a maximum for that crop. An apparent crop coefficient may be derived from remotely sensed data using reflectance and emittance properties of the vegetated surface in contrast to the present tedious methods of obtaining crop coefficients.

Water Budget

A water budget is frequently used to estimate water used in evapotranspiration over a specific time interval. The water conservation equation for a volume of plant root zone for a specific time period is

$$P + I = R + \Delta W + E + T + D \qquad [10]$$

where P is the precipitation, I is irrigation, R is surface runoff, ΔW is the change in stored water in the soil volume during the time interval, E is evaporation from soil, T is transpiration from the plants, and D is the amount of soil water either entering or leaving the soil volume. The precipitation, irrigation, runoff, and change in storage terms are readily measurable. The profile drainage, evaporation, and transpiration terms are more difficult to measure.

Between rainfall or irrigation applications, the terms P, I, and R will equal zero. The water conservation equation then becomes

$$-\Delta W = E + T + D \qquad [11]$$

with the terms previously defined. The change in water storage (ΔW) is measured as profile water content at the end of the time period minus profile water content at the beginning of the period. Equations (10) and (11) are both in the integral form with the terms being totaled over a given period of time. It is often desired to speak of water loss as a rate, or loss per unit of time. Equation (11) expressed in differential form becomes

$$-dW/dt = dE/dt + dT/dt + dD/dt \qquad [12]$$

where W is the water storage in the soil volume and t is time. Equation (12) is the time rate of change form of the water conservation equation between water applications. The rate of evaporation from soil (dE/dt) and the rate of transpiration from plants (dT/dt) are combined to form

the evapotranspiration (ET) rate term. The rate of profile water drainage (dD/dt) is commonly referred to as the soil water flux (v). Equation (12) takes the form

$$-(dW/dt) = ET + v \qquad [13]$$

where (dW/dt) is the rate of water storage change in the soil volume.

The flux term in equation (13) can be estimated using Darcy's equation

$$v = Ki \qquad [14]$$

where v is the soil water flux, K is the unsaturated hydraulic conductivity, and "i" is the hydraulic gradient or the driving force. This computation requires considerable ground information, which is difficult to derive and for large areas is economically infeasible.

When the water budget is used, neglect of terms describing water loss other than evaporative flux may introduce considerable error. For example, Black, Gardner, and Tanner (1970) determined on a field water budget study that during a 60-day study period the total water loss from a field of snap beans was 35 cm with 17 cm lost to ET and 18 cm lost due to drainage from the 150-cm profile. Goltz et al. (1971) found that for an onion crop, the drainage loss exceeded the ET loss. Therefore, the water budget approach is only applicable where a considerable knowledge of the landscape physical properties and the groundwater status is known. If the crop canopy and fallow soil surfaces are an indicator of the surface and subsurface moisture at the time of measurement, the errors in the traditional water budget would not be present where the estimation of soil moisture occurs at a point in time by remote sensors which would directly determine the stored soil water.

Remote-Sensing Applications to Soil Water-Evaporation Assessments

When the supply of water to the evaporating surface (primarily through conduction through the soil matrix to the fallow soil surface or translocation through plant roots and tops to the leaves) is limited, the evaporation rate decreases with a subsequent increase in temperature of the evaporating surface. In early work, Tanner (1963) used energy balance relationships to show that if the transpiration rate of plants decreased and if the radiation balance and wind structure remained the same, the decrease

in latent heat exchange resulted in an increased plant temperature. The incoming energy to the surface was utilized in heating the surface with dissipation by sensible and soil heat flux in contrast to being partitioned into latent energy with subsequent dissipation as latent heat flux. As moisture stress increases, with consequent decreases in ET rate and increases in surface temperature, the relative turgidity of the plant decreases. Wiegand and Namken (1966) observed in cotton plants that a decrease in relative turgidity of plants from 83 to 59% resulted in a 3.6 C increase in leaf temperature. This magnitude of temperature variation is well within the resolution capabilities of modern remote-sensing systems. Moore et al. (1974) illustrated that the X/5 thermal detector on the S192 of SKYLAB had sufficient thermal resolution to detect emittance variations which were associated with soil moisture related terrain features in vegetated landscapes.

Werner and Schmer (1972) investigated the application of remote sensing techniques to the inventory of soil water in croplands and rangelands. In addition to data from several film-filter combinations within the reflective region, thermal scanning data were collected. They concluded that the blue region of the electromagnetic spectrum could be used for determining soil water conditions with little or no crop cover. The green, red, and near-infrared regions were all useful for evaluating soil water where crop or range canopies were present. Their evaluations were conducted within specific agricultural land uses. The reflectance differences among crop types are considerable and vary with phenological stage; therefore, the reflective spectral region has limited use for predicting moisture variation within diverse agricultural regions. Since water has a considerable affect on the energy budget, surface emittance variations may provide a better estimate of soil moisture less influenced by crop cover. Idso, Jackson, and Reginato (1975) have presented a comprehensive discussion of the detection of soil moisture on fallow land. They illustrated the use of a predicted moisture tension in contrast to absolute moisture quantity to reduce the variation among soil types.

TEST SITE IDENTIFICATION

Test-site Selection Procedure

Many test sites were selected for anticipated data collection during the SL-2, SL-3, and SL-4 missions. Site selections were made by the investigators and personnel familiar with the area by evaluation of historical LANDSAT and aircraft imagery and by field reconnaissance surveys. After initial site selection, a general field survey was conducted by on-site ground inspection. The criteria for site selection included the following: uniform soils, a diversity of agricultural land uses, the occurrence of irrigated crop and fallow fields with dryland of similar land use in adjacent areas, and landowner approval. Since energy budget information was of primary interest, thermocouples and heat flux plates were placed in the soil at various depths to 100 cm. The minimum time required for implanting the sensors prior to measurement was 24 hours or one diurnal cycle. Therefore, considerable travel to potential test sites with detailed inspection was required, especially during SL-3 when the workshop was not in a stable orbit.

Description of Carrizo Springs Test Site

The site near Carrizo Springs, Texas (28° 30'N, 99° 50'W), was selected in accordance with the estimated coverage of the S-192 scanner and with the general criteria previously listed for test site selection. The soils were predominantly of the Uvalde-Montell-Atco Association and are nearly level to gently undulating, deep, silty clay loams, clays, and clay loams that have moderately and very slowly permeable subsoils (Soil Conservation Service, 1972). An image of SKYLAB S190-B color-infrared photography (Fig. 1) includes the test site and surrounding area. The predominant land use was range with some fields of irrigated agriculture, including alfalfa, cabbage, onions, carrots, spinach, and pre-irrigated fallow. The dryland agriculture included fallow, improved range, and unimproved range. Thirty separate fields identified in Fig. 2 for which ground data were acquired were typical of the regional land-use and soil moisture variations. Area "9" was a surface water body. A frost had occurred approximately one-month prior to the SKYLAB overpass; therefore, the dryland agriculture was essentially dormant.

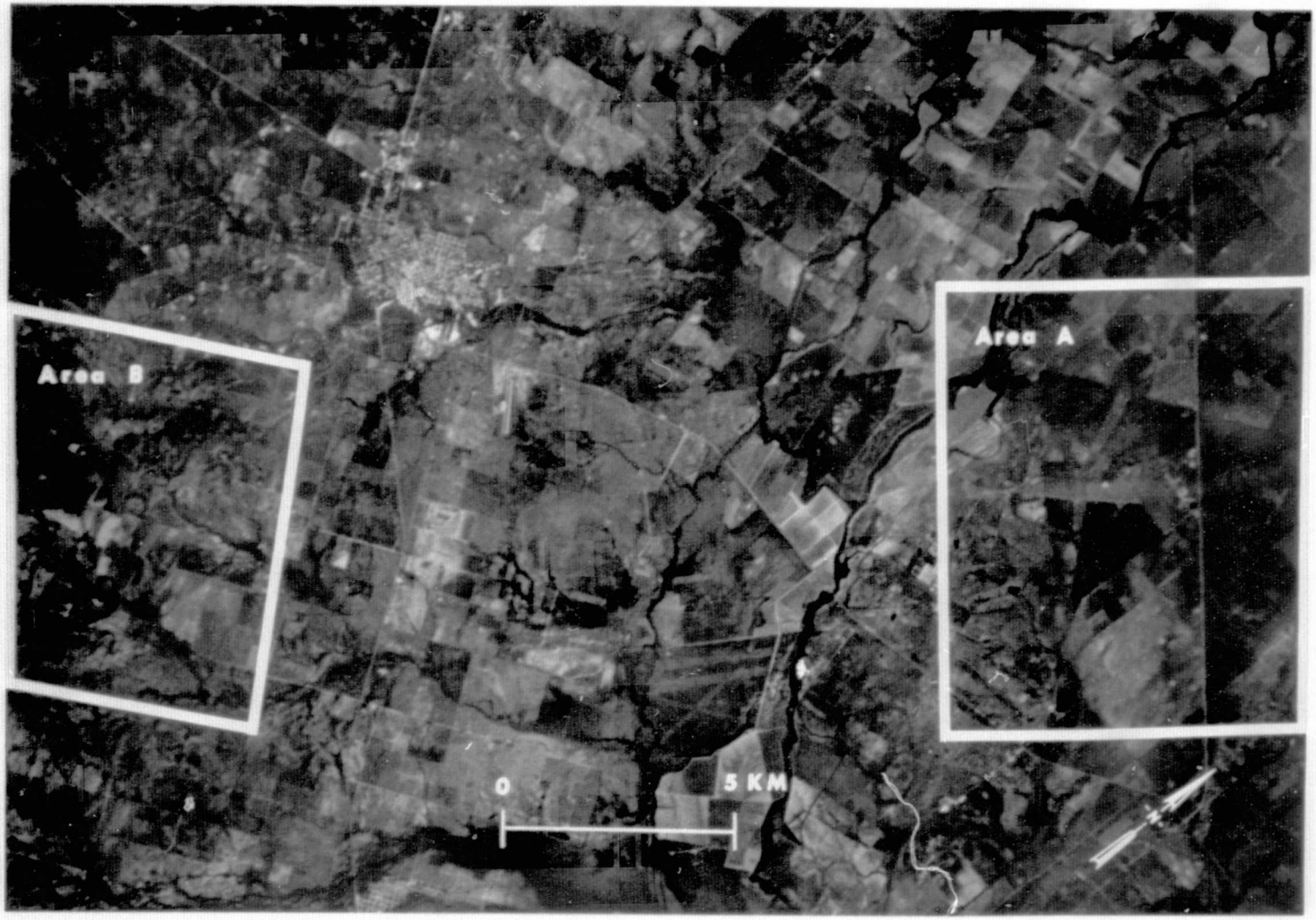

Fig. 1 - A print of S190-B color-infrared photography acquired over the Carrizo Springs test site (orbit 94, ground track 20). The two regions of intensive data collection are denoted and are represented in Figs. 2a and 2b using larger scale data (original in color).

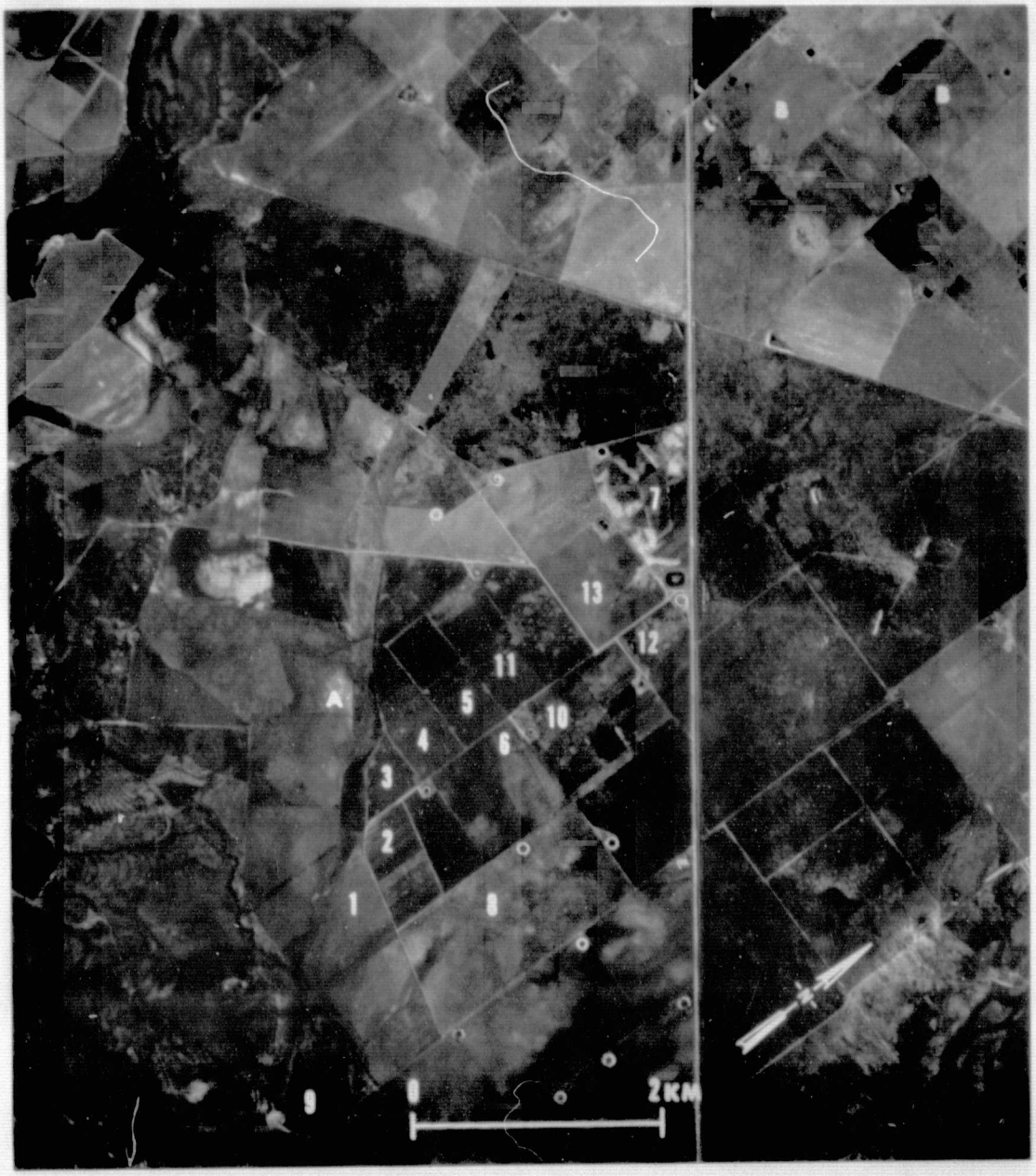

Fig. 2a - Area A

Fig. 2 - Color-infrared photograph illustrating the two intensive test sites near Carrizo Springs, Texas. Data are from RB-57F NASA mission 260, RC-8 "6-inch" focal length camera at 18,300-m AGL. Refer to Table 1 for description of land use and soil moisture for fields as numbered. Area "A" is a seep and areas "B" are center pivot irrigation systems (original in color).

Figure 2 (continued)

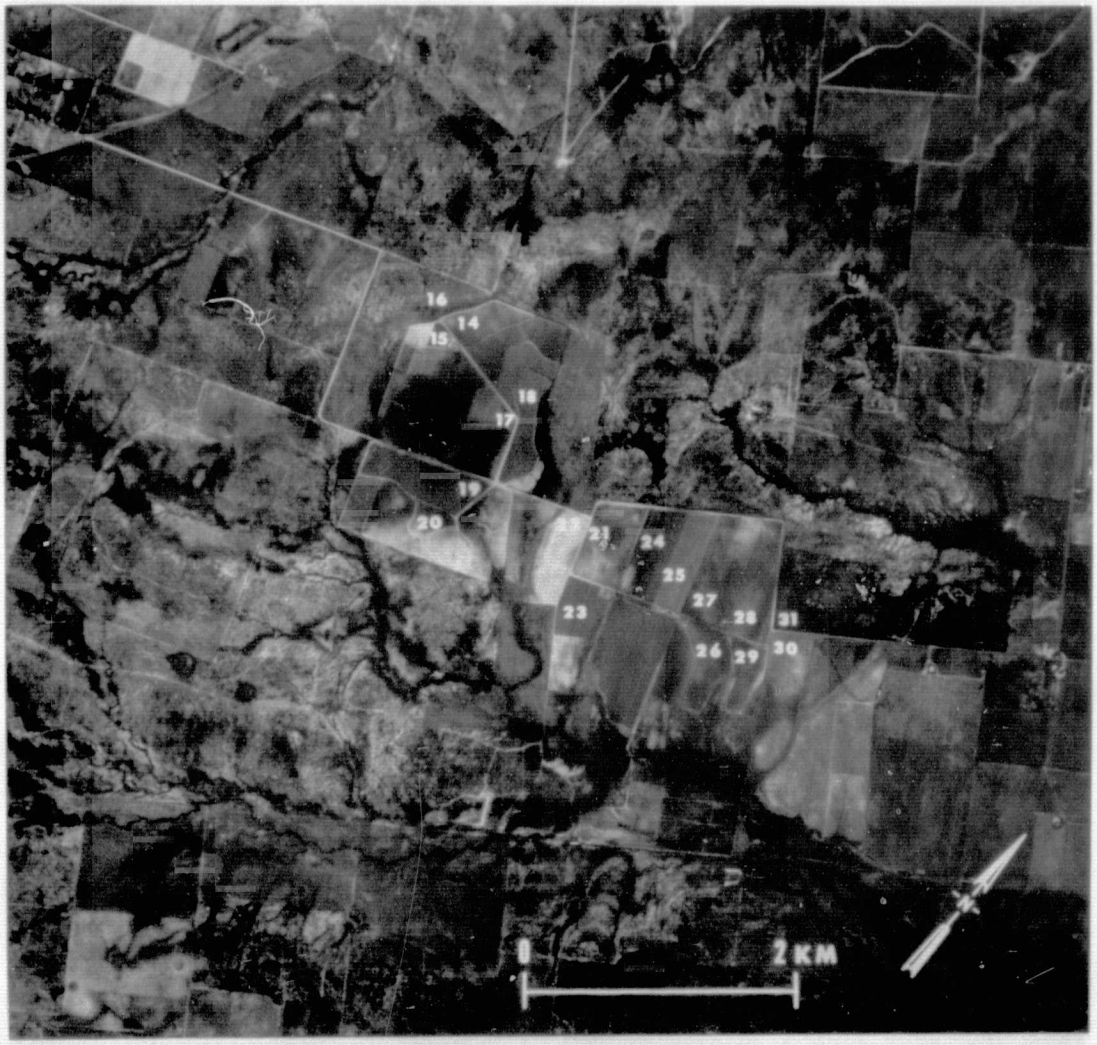

Fig. 2b - Area B

DATA COLLECTION

Ground Data

Ground-based energy budget data were acquired for specific fields within the test site. Measurements included thermocouple soil temperatures at several depths, air temperature and vapor pressure at several heights, net radiation, filtered radiometry, and soil heat flux. A description of the sensors and their placement is in Table A-1 of Appendix A. Only those measurements required for the specific evaluations in this document are presented. Land-use and soil moisture data were acquired to characterize the thirty agricultural fields. Proportions of green vegetation, fallow, and dry organic debris were determined from slides and are reported as percent of total area. Slides were exposed using a hand-held 35-mm camera vertically 1-m above ground level (AGL) over the test site. Measurements were conducted by projecting slides on a grid containing 100 randomly placed dots. Each value was reported as the mean of four separate observations on each of three replicate slides for each field. Soil moisture samples were collected in triplicate with each sample composed of two subsamples. The percent gravimetric soil moisture was determined for the 0→2 cm, 2→10 cm, and 10→30 cm depths by oven drying at 105 C. A composite value for the 30-cm profile was computed by weighting and summing the averages for the depths represented.

The locations of the two primary areas of ground data collection are identified on the S190-B data in Fig. 1. The intensive test fields are numbered on prints of aircraft data presented in Fig. 2. Table 1 is a summary of the ground data with field numbers corresponding to those in Fig. 2.

Aerial Data

A multistage data collection mission was accomplished including NC-130B, RB-57F, and SKYLAB data. The various operable sensors of each platform along with delivered data products are described in Table A-2 (Appendix A). The mission numbers include: 258 for NC-130B, 260 for RB-57F, and orbit 94 on ground track 20 at 20:12 GMT (13:12 local CST) on 28 January 1974 for SKYLAB. The S-192 scanner aboard the SKYLAB workshop used the X/5 thermal detector for this pass.

TABLE 1. LAND USE AND SOIL MOISTURE OF AGRICULTURAL FIELDS WITHIN TEST SITE

Field No.[1]	Crop	% Green[2]	% Gravimetric Soil Moisture			
			0→2cm	2→10cm	10→30cm	Composite
1	range	1.2	11.33	16.24	15.06	15.13
2	onions	28.0	11.96	19.14	18.50	18.23
3	alfalfa	22.8	14.74	18.50	12.53	14.27
4	alfalfa	86.8	35.21	25.38	22.94	24.41
5	alfalfa	86.1	23.36	19.97	18.08	18.94
6	fallow	0.0	8.72	20.23	24.81	22.52
7	fallow	2.6	32.86	31.98	28.17	29.50
8	fallow	0.0	12.42	21.50	19.00	19.23
9	water					
10	fallow	6.0	27.05	26.67	24.99	25.57
11	alfalfa	89.2	31.90	23.67	23.17	23.91
12	alfalfa	10.3	15.63	21.09	13.82	15.88
13	fallow	0.0	11.40	20.98	18.26	18.53
14	cabbage	30.5	5.81	12.67	14.77	13.61
15	onions	11.6	3.77	11.11	12.50	11.55
16	range	1.2	5.47	9.04	8.18	8.23
17	cabbage	10.3	10.93	14.83	15.95	15.32
18	cabbage	82.1	9.23	13.00	10.73	11.24
19	cabbage	85.0	16.74	20.32	22.24	21.36
20	onions	10.6	9.20	18.76	19.89	18.88
21	onions	1.2	6.78	13.55	14.80	13.93
22	fallow	0.0	2.64	10.95	10.94	10.39
23	carrots	71.2	11.15	12.90	13.86	13.42
24	cabbage	37.6	22.66	22.71	22.13	22.32
25	cabbage	55.8	12.44	21.74	21.59	21.02
26	fallow	0.1	9.53	22.29	23.00	21.91
27	fallow	0.0	5.95	16.82	13.85	14.12
28	carrots	62.0	9.04	18.11	20.93	19.39
29	carrots	22.6	4.93	13.97	16.14	14.81
30	fallow	0.2	4.33	14.56	15.30	14.37
31	range	0.0	7.01	11.97	10.55	10.69
A	seep					
B	center pivot irrigation					

[1] Refer to Figs. 2a and 2b for field locations.

[2] Reported as percent of total area which was green vegetation when viewing the surface vertically.

PROCEDURES FOR DATA REDUCTION

General

Visual and statistical analyses were conducted on the data. Visual analyses of the scanner data were possible using screening film products from the scanners and using the DAS analysis system at NASA, JSC. Statistical analyses of digital scanner data were conducted on unrectified products from the NC-130B and SKYLAB scanners. Film products from the RS-7 scanner aboard the RB-57F aircraft and the S190-A film from SKYLAB were digitized using the scanning microdensitometer (Signal Analysis and Dissemination Equipment - SADE) at the Remote Sensing Institute. Location and statistical analyses of the thirty individual fields were conducted by: applying an edge detection algorithm to locate radiometrically homogeneous areas within the digital matrix, computing means and standard errors of the radiance values within each area, and testing on a field-by-field basis the field means for each spectral region using a t-test at the 0.05 confidence interval.

Edge Detection

Since the original S192 scanner data were in a conical form, recognition and accurate mapping of field boundaries in the digital data were difficult. Therefore, an algorithm was developed to locate edges between relatively homogeneous areas in a matrix of digital data. The assumptions in the algorithm included:

1. An ideal edge between two homogeneous data clusters occurs at a step change in the data.
2. The rate of change of data values (gradient vector magnitudes) within a homogeneous area is small.
3. The gradient magnitude near and at an edge is greater than within a homogeneous area.
4. The gradient vector direction at an edge is perpendicular to an edge.
5. An edge point has the maximum gradient value when compared to adjacent points in the gradient vector direction.

A general flow chart of the algorithm is presented in Fig. 3. The magnitude $|F(x,y)|$ and the direction (θ) are computed for each point by

$$\theta = \arctan\left(\frac{\partial F}{\partial Y} \Big/ \frac{\partial F}{\partial X}\right) \quad [15] \qquad |F(x,y)| = \left[\left(\frac{\partial F}{\partial Y}\right)^2 + \left(\frac{\partial F}{\partial X}\right)^2\right]^{1/2} \quad [16]$$

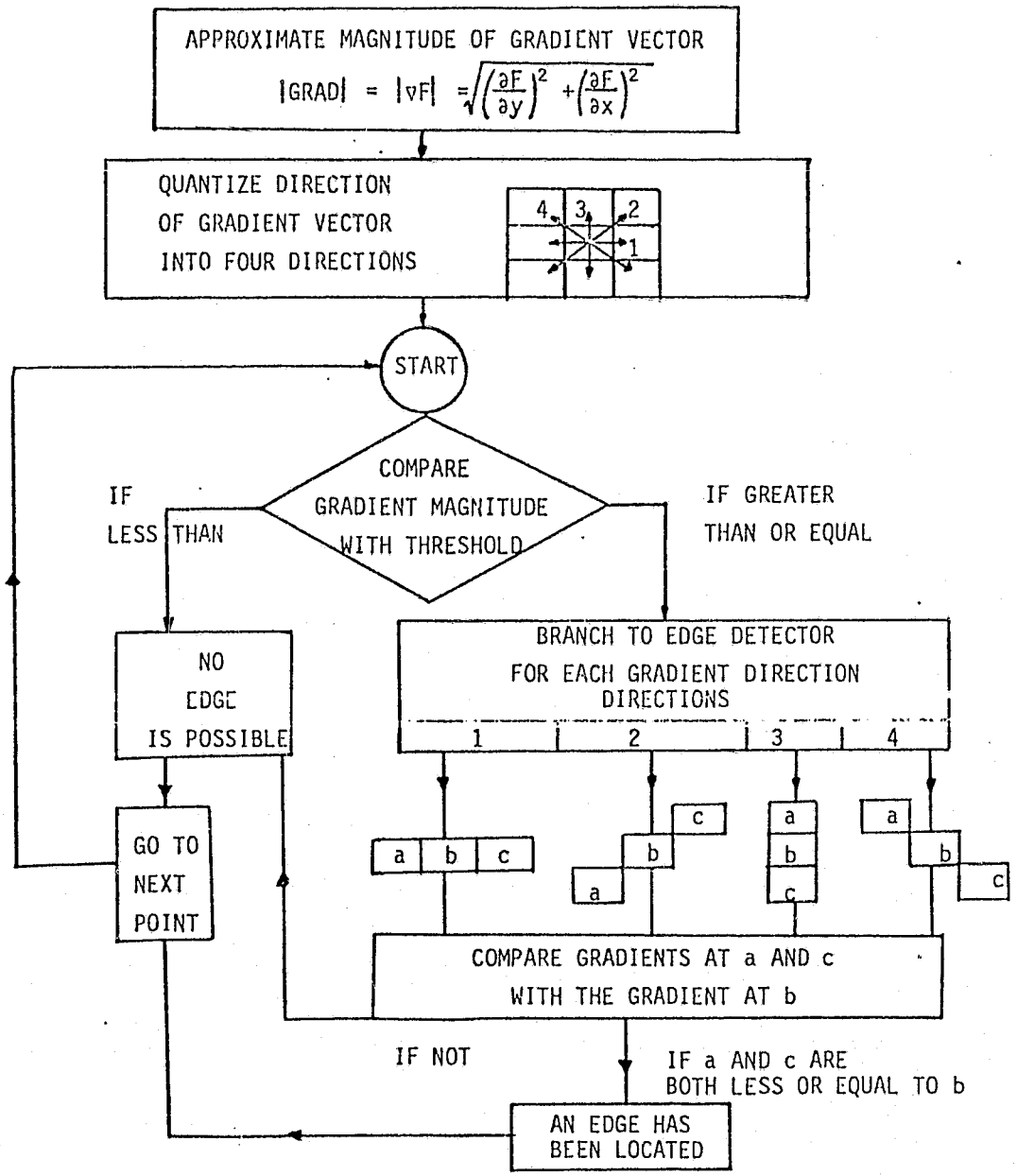

Fig. 3 - Flow diagram of edge detection procedure which was applied to matrices of digital data.

The orthogonal derivatives $\frac{\partial F}{\partial X}$ and $\frac{\partial F}{\partial Y}$ are approximated at the midpoint of four data points with the two numerical differences across the diagonals of the points. The gradient is quantized into four discrete directions illustrated in Fig. 3. For example, direction one occurs when the gradient direction has a numerical value in the range of 22.5° to -22.5° or 157.5° to 202.5°.

After initial computation of the gradient vector direction and magnitude, the edge detection algorithm is applied. For each separate data point, the gradient magnitude is compared to a threshold value. If the value is less than the threshold, the data point is not a potential edge point and the algorithm goes to the next point. If the gradient value is greater or equal to the threshold, the point is retained for further analysis. The gradient vector direction is perpendicular to an edge. An edge is located by comparing adjacent gradient vector magnitudes in the gradient vector direction. The four possible gradient directions are illustrated with data points a, b, and c in Fig. 3. An edge is located at point "b" when the gradient magnitudes at both adjacent points "a" and "c" in the gradient vector direction are smaller than the gradient magnitude at point "b". If this condition is not met the algorithm returns and goes to the next point. Edge points are coded with the gradient magnitude at that point and other non-edge points are coded as zeros. A listing of a Fortran program that implements the edge detection algorithm is included in Appendix B.

Adjacency Method

An algorithm called the adjacency method for separation of regions of near-homogeneous radiometric data was developed. The algorithm computes statistics including the number of observations, sum of data values, and sum of squares of the data values for all separate data regions. In general, the algorithm uses the following assumptions:

1. Gradient magnitudes within near-homogeneous data regions (agricultural fields for these data) are smaller than near edges between regions.
2. Edges are approximated by gradient magnitudes greater or equal to a gradient threshold.
3. All data points which are smaller than a gradient threshold belong to near-homogeneous data regions.

4. All data points that are surrounded by an edge and are adjacent belong to one and only one data region.

A flow chart of the procedure is in Fig. 4. In general, the gradient magnitude is computed for each data point and a threshold is applied. Those data points whose gradient magnitudes are larger than the threshold value are regions where edges occur. The adjacency method assigns the same numbers to all separate data regions which have gradient magnitudes less than the gradient threshold and are surrounded by edges. Statistics are computed for each data region using the original radiometric values.

The gradient threshold is chosen in a similar manner to that for the edge detection algorithm. The magnitude of the gradient threshold should be sufficiently large to eliminate noise which creates false edges but yet retains major edges. The Fortran program which implements the adjacency method is included in Appendix B. The resulting statistics computed using the adjacency method are analyzed with a classifier described in the next section.

Statistical Classifier for Field Comparison

Statistical means and variances for each separable field were computed using the adjacency method. Separable fields were those identified either by the adjacency method or by an artificial line placed in the data where field boundaries were known but were not located using the adjacency method. A two-tailed t-test was used to determine which field means were statistically separable. A flow chart for the procedure is in Fig. 5 and a listing of the Fortran program is in Appendix B. Means within a spectral band were ranked and statistically compared. Classes of data were generated by combining statistically similar means (at 0.05 confidence level) into grand means. Resultant data classes were statistically separable using the two-tailed t-test at the 0.05 significance level. The two-tailed t-test (in contrast to the one-tailed t-test) was used to reduce bias because of the initial ranking of the means. Orthogonality was maintained because each mean was used only once. If the mean was statistically separable from the adjacent mean, it was put into a separate class. If there was no statistical difference at the 0.05 level, original data values for the mean were combined with data values for the adjacent mean resulting in the computation of new statistics

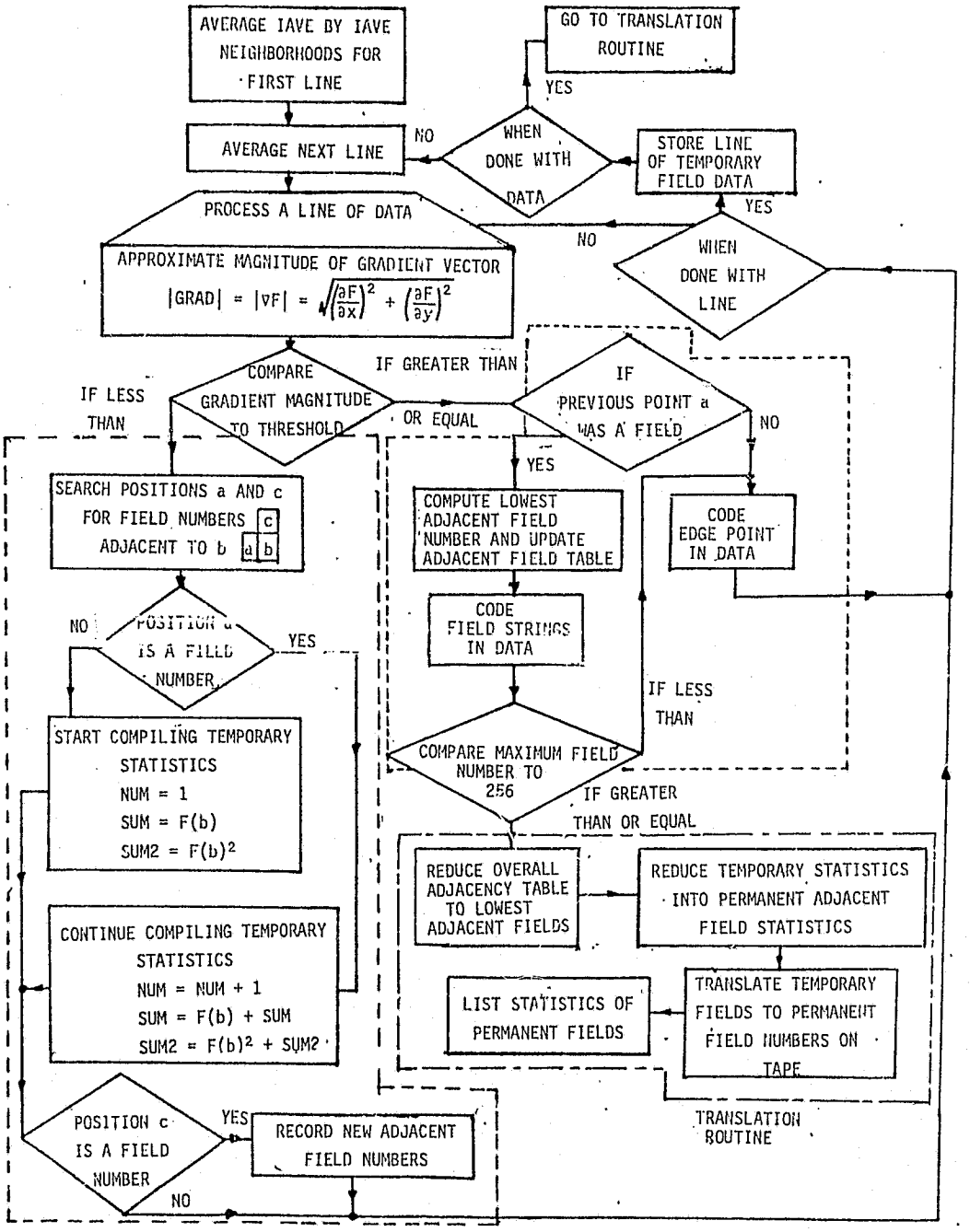

Fig. 4 - Adjacency method flow chart.

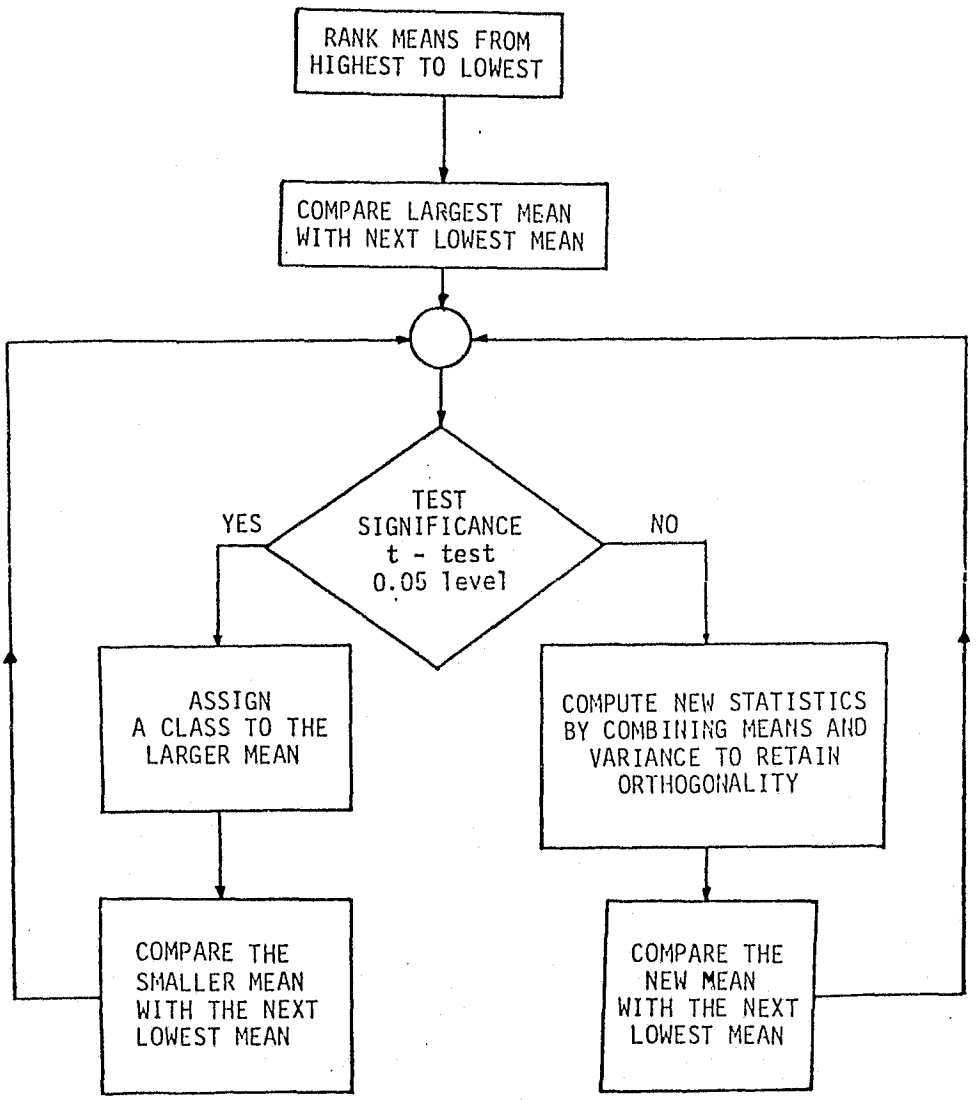

Fig. 5 - Flow diagram of the t-test procedure.

for subsequent comparison.

Example Output

Figure 6 is an example of the original analog film data from the RS-7 scanner of the RB-57F, a gray-level SADE map prepared by quantization of the 256 output codes of the digitized film data, an edge detection map, and an output from the adjacency method. Field numbers correspond to those in Fig. 2a and Table 1. Note that the fields which had no apparent emittance variations were not separable with boundary detection or adjacency classifier (eg., #12 and 13). An artificial boundary was placed between those two fields and statistics were hand computed using the values of data listings from the tape.

SKYLAB S190-A

The black and white positive transparencies and appropriate gray-scale wedge calibration strips from the S190-A were digitized into 256 gray levels via SADE. The film/filter combinations for each station are in Table 2.

TABLE 2. FILM FILTER/COMBINATIONS FOR CAMERA STATIONS FOR THE S190-A.

Position	Film Type	S190-A Filter	Wavelength in μm
1	2424	CC	0.7→0.8
2	2424	DD	0.8→0.9
3	So-022	BB	0.6→0.7
4	So-022	AA	0.5→0.6

The output of the digitizer operated in log mode was codes ranging from 0→255. These output codes were translated into corresponding film densities of the duplicate sensitometry strips. Using procedures described by Lockwood (1974), densities were calibrated to the originals with subsequent calibrations to input radiance levels in cal cm^{-2} min^{-1}. The edge detection, adjacency method, and t-test algorithms were applied to the data to reduce and statistically classify the 30 fields.

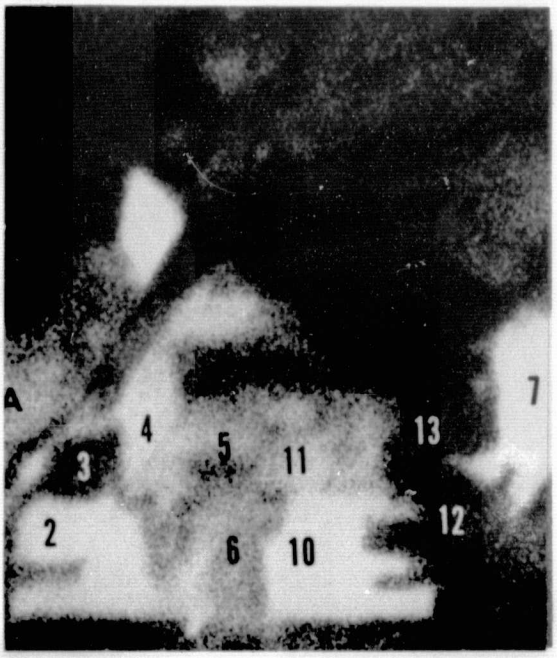

a. RS-7 thermal scanner film, Approximate scale 1:32,500 (light is cool)

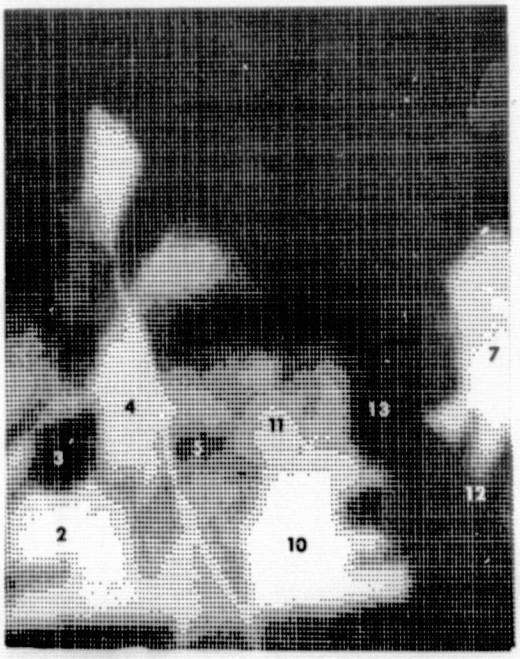

b. Overstrike printout of SADE values (light is cool)

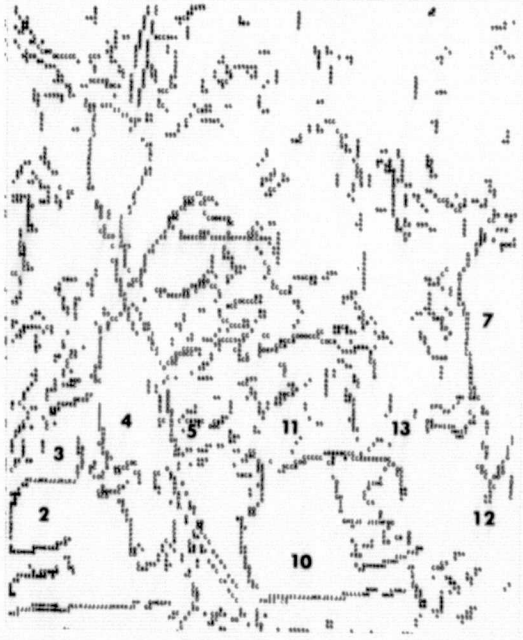

c. Edge detection.

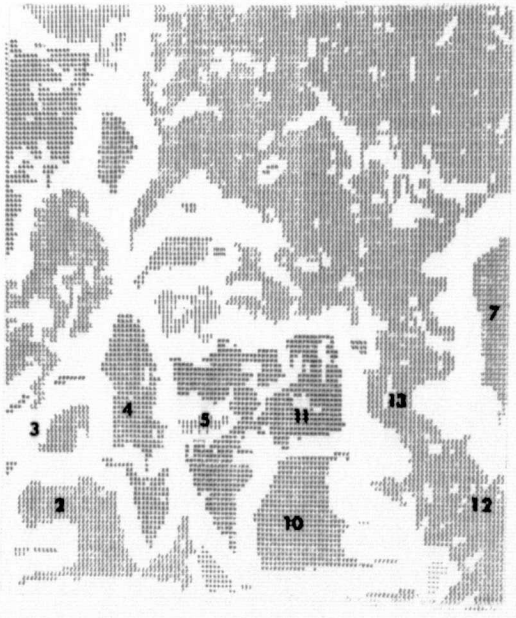

d. Adjacency method.

Fig. 6 - Example outputs of processing algorithms. Field numbers similar to those in Fig. 2a and Table 1.

SKYLAB S190-B

The color-infrared film from the S190-B mapping camera was used as a base map for analyses of digital products.

SKYLAB S191

The S191 data were acquired over Delta Lake Site 390. Forward look angles were not affected by clouds but backward look angles had cloud interference. An evaluation of the S191 data was conducted to determine the angular effects of sensor-measured radiance in the various S192 wavebands. The radiance variations included varying thicknesses of the atmospheric and geometric variations in sensor→target→sun angles.

A plot of original data calibrated to radiance (Juday 1974) versus wavelength for the normal-to-horizon (0°) look angle was prepared. In addition, variance of the radiance measured at the detector which was associated with differing atmospheric path lengths and target-to-S191 look angles was evaluated. The data take required 1 minute and 9 seconds. Sensor drift of ≈0.15% per minute did not significantly affect the comparison of radiance measurements within the small observation time; however, absolute radiance may have been in error because the actual timing of the prepass autocal was not known. The relative atmospheric path was determined by geometrical configuration of the SKYLAB workshop to the location of the ground target. The shortest atmospheric path was at nadir and was given a zero length. The longest path for the SKYLAB altitude was 149 km greater than the assumed zero path. The 149-km length was calculated by assuming that atmosphere extended to the altitude of the SKYLAB which, of course, is not true. However, the relative radiance changes from normal in percent of total length are not affected by this assumption. A regression analysis of the relative path length to radiance was performed.

SKYLAB S192

Visual analyses of the DAS products from the S192 scanner were performed to identify which available spectral regions could be used to identify water-related soil variations. Digital analyses were completed including application of the edge detection and adjacency method algorithms for field location and computation of statistics, calibration of the

data to radiance, and correlation and regression of radiance data to ground variables. The t-test procedure was used to determine which fields were separable within each spectral region. The Channel 15-16 thermal data were used in preparation of an evapotranspiration map. Specific assumptions used in developing the map will be outlined when the map is presented later in this document. The spectral regions available for analyses are presented in Table 3. The X/5 detector was operative in the scanner during this period and this deleted some of the channels available for data acquisition. In addition, the channel 11 data were not suitable due to noise.

TABLE 3. SPECTRAL REGIONS AVAILABLE FROM THE S192 SCANNER.

Channel Number	Spectral Region in μm	High or Low Rate
3-4	0.56-0.61	high
7-8	0.68-0.76	high
9-10	0.78-0.88	high
19	0.98-1.08	low
20	1.09-1.19	low
12*	1.55-1.75	high
13-14	2.1-2.35	high
15-16	10.2-12.5	high

* Channel 11 not suitable for analysis

SKYLAB S193

No S193 data were received for the test site.

SKYLAB S194

Due to the resolution of S194 and the small test site, the S194 data were not analyzed.

RB-57F Aircraft

Aircraft data acquired during this investigation are listed in Table A-2, Appendix A. Photographic products were used for positive ground identification and illustration. Thermal data from the RS-7 scanner were visually interpreted to aid in identifying within-field variations which were below the resolution of the S192 sensor aboard SKYLAB. In addition,

data processing algorithms were initially tested on the SADE digital product of the RS-7 thermal analog film. Example products were illustrated in Fig. 6.

NC-130B Aircraft

Screening film from the multispectral scanner was visually and digitally evaluated to reinforce interpretations of water-related terrain variations observed using the SKYLAB data. The NC-130B and SKYLAB S192 data provided multistage, multispectral data for concommitant analyses.

DATA PRESENTATION AND VISUAL INTERPRETATION

Ground Data

Soil moisture measurements and land-use descriptions for each of the 30 fields were presented in Table 1. A correlation analysis between means of ground measurements and of spectral radiance for the thirty fields was conducted. The simple linear correlation coefficients are listed in Table 4. Soil moisture contents at the various depths were all highly correlated. The only significant correlations of land use and soil moisture were between both percent green vegetation and percent fallow with 0→2 cm soil moisture. However, only 21% of the variation in 0→2 cm moisture could be accounted for with percent green vegetation and 14% with percent fallow. Several fallow fields were being irrigated in preparation for planting small grain. Many fields of vegetable crops were mature and were being harvested. These two conditions probably decreased correlations. However, the ground conditions did provide a test site favorable for determining the utility of reflectance and emittance data for assessing actual soil moisture variations without the interference of a high correlation between soil moisture and vegetation conditions.

SKYLAB S190-A

The four separate black and white S190-A images which were digitized for statistical analyses are presented in Fig. 7.

SKYLAB S190-B

The S190-B color-infrared photography (Fig. 1) was used as a base map. Accurate location and mapping of field boundaries were derived from these data.

SKYLAB S191

Radiance versus wavelength was plotted in Fig. 8 for the 0° (nadir) look angle. Note that the scale of the vertical axis differs by a factor of 100 when comparing the reflective (Fig. 8a) and the thermal (Fig. 8b) spectral regions. The approximate spectral regions of S192 data are noted. The target scene was range vegetation and was not ground inspected due to its distance from the intensive test site. The S191 land region was not within the coverage of the S192 sensor.

TABLE 4. CORRELATION OF GROUND VARIABLES.

	Gravimetric Soil Moisture				Land Use		
	0→2cm	2→10cm	10→30cm	Composite	% Green Vegetation	% dry debris	% fallow
Soil moisture							
0 → 2cm	1.000						
2 → 10cm	0.822**	1.000					
10 → 30cm	0.666**	0.881**	1.000				
Composite	0.783**	0.952**	0.980**	1.000			
Land use							
% green vegetation	0.461*	0.157	0.198	0.228	1.000		
% dry debris	-0.031	-0.144	-0.328	-0.259	-0.173	1.000	
% fallow	-0.373*	-0.035	0.055	-0.017	-0.737**	-0.537**	1.000

where * is significant at the 0.05 level and ** is significant at the 0.01 level. 28df

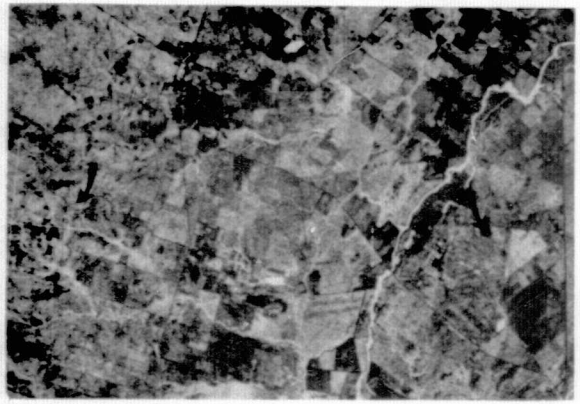

a. 0.5 → 0.6 μm
Station A-6

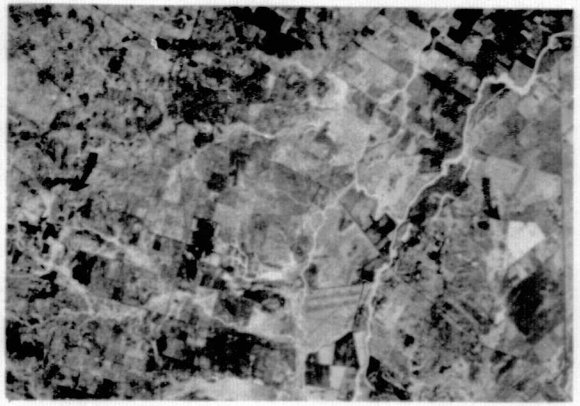

b. 0.6 → 0.7 μm
Station A-5

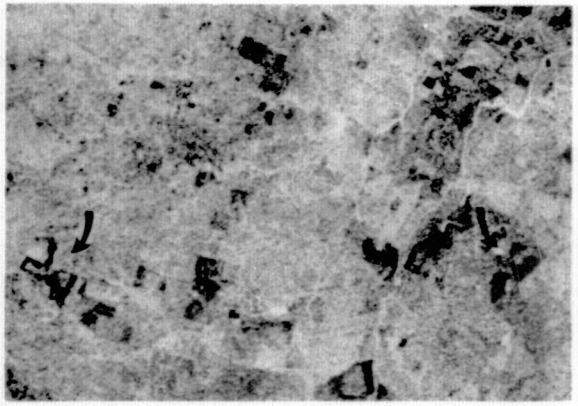

c. 0.7 → 0.8 μm
Station A-1

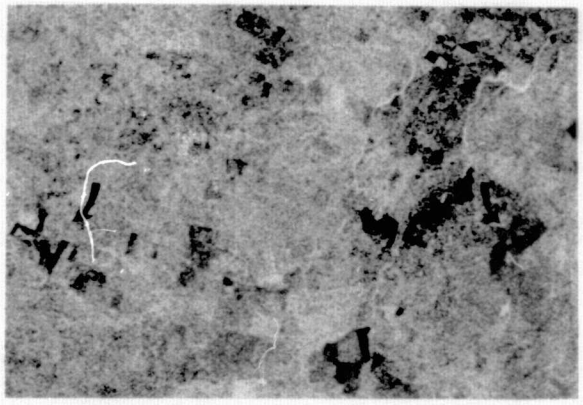

d. 0.8 → 0.9 μm
Station A-2

Fig. 7 - Negative prints of S190-A data which were digitized to statistically analyze the 30 field test sites. Area is similar to that of S190-B presented in Fig. 1. Arrows point to intensive test sites identified in Figs. 2a and 2b.

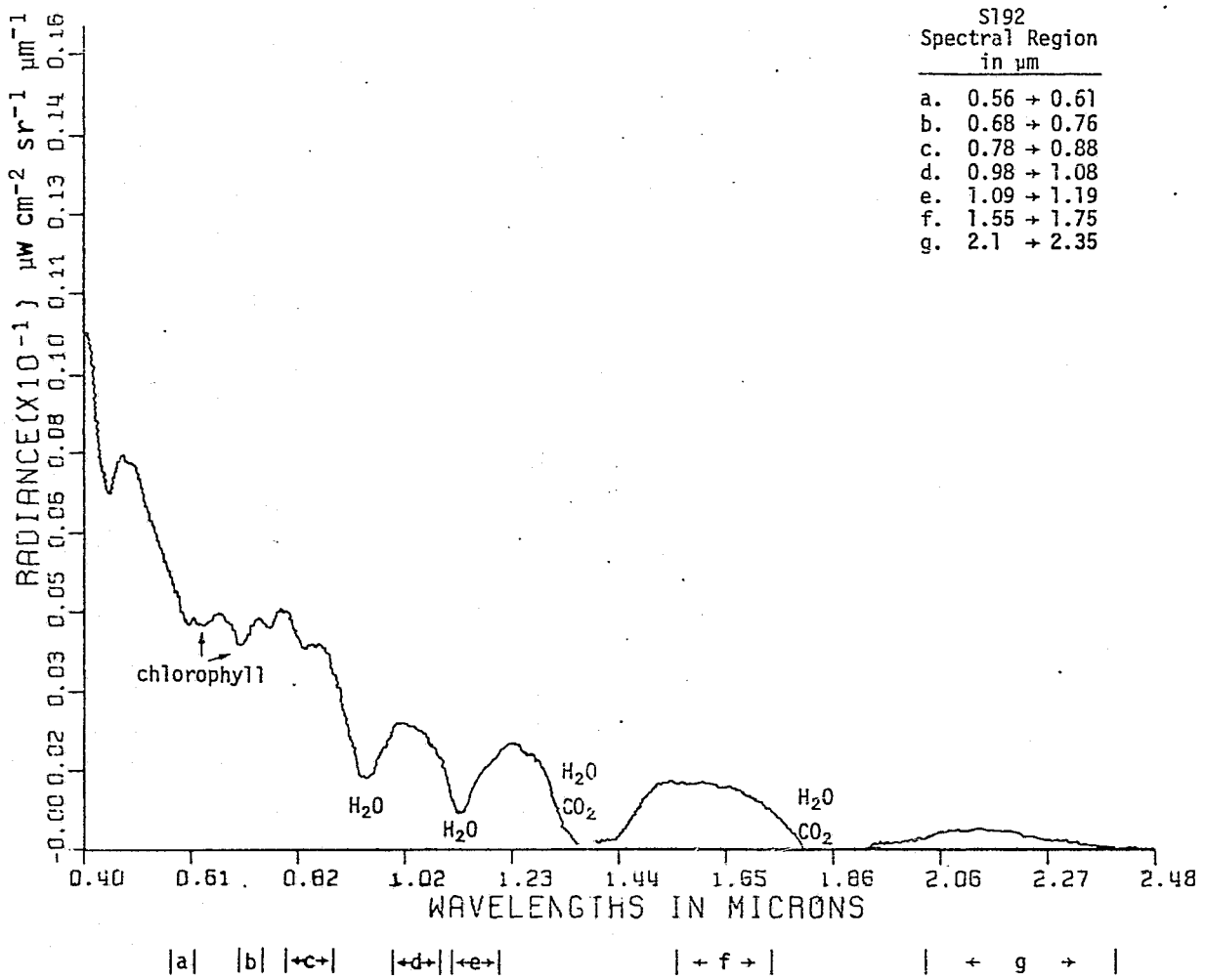

Fig. 8a - reflective

Fig. 8 - Plot of radiance versus wavelength as measured by the S191 at the 0° look angle. The major atmospheric absorption bands and S192 spectral regions are noted.

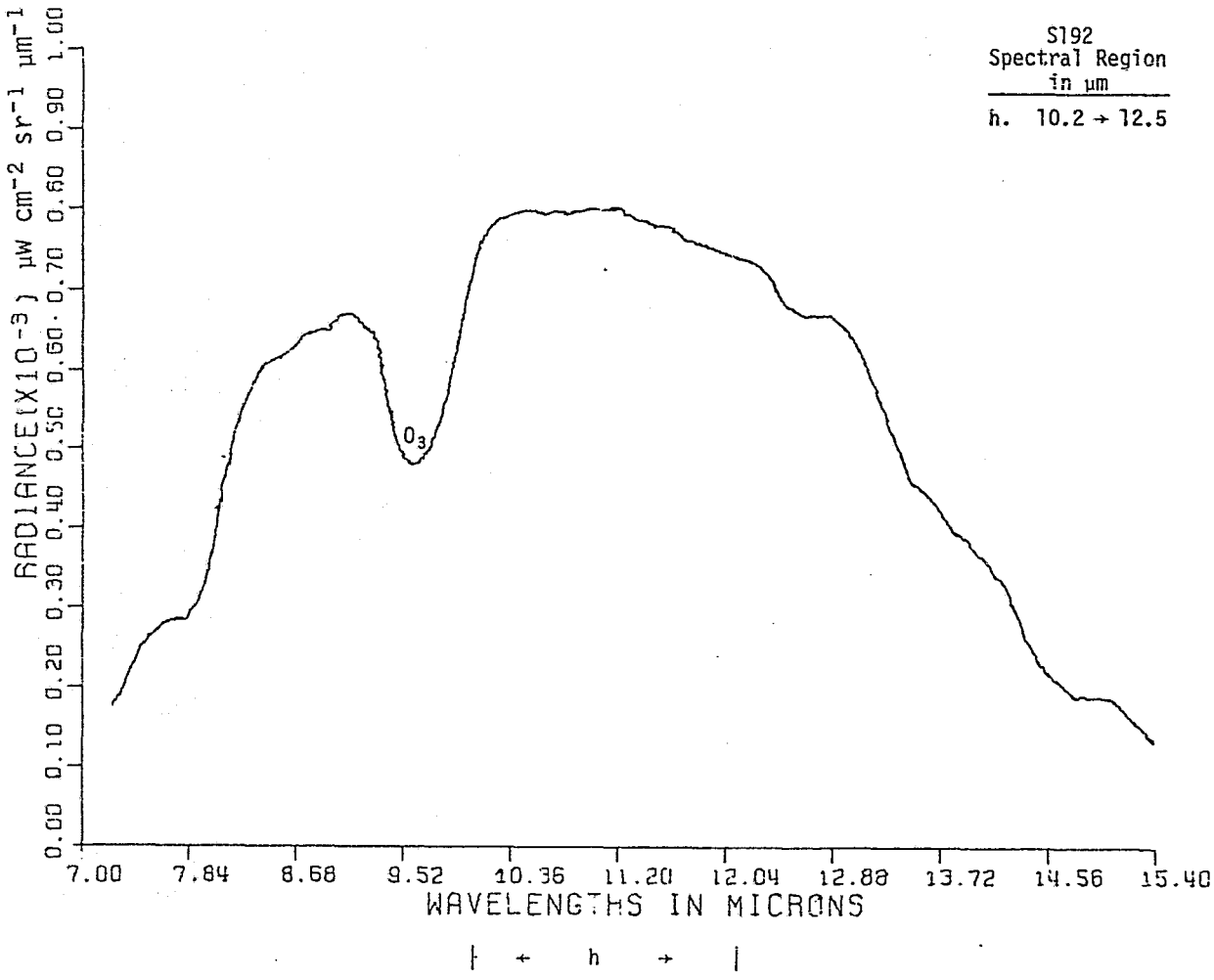

Fig. 8b - thermal

(Fig. 8 continued)

The various water, carbon dioxide, and ozone absorption bands are noted in Fig. 8 and are evident in the measured radiance values. The chlorophyll 'a' and 'b' secondary absorption bands are evident and appear appropriately at 0.660 μm and 0.642 μm, respectively. The ozone absorption band (9.4→9.8 μm) in the thermal region is present.

SKYLAB S192 and Multispectral Data from the NC-130B and RB-57F

The DAS display products of SKYLAB S192 data are presented in Fig. 9. The area is similar to that in Fig. 2a with the same field number annotations. Screening film from the multispectral scanner of the NC-130B is in Fig. 10. The scanner aboard the NC-130B did not cover the center pivot irrigation systems; however, the RB-57F mission in Fig. 11 did image the center pivots.

The twelve separate agricultural fields are labeled in Figs. 9→11. In addition, two center pivot irrigation systems were located and labeled "B" in Figs. 9 and 11. Ground data on land use and soil moisture were not acquired for the two areas. However, upon detailed inspection of the low-altitude NC-130B photographic data, the center pivots were assumed to be operative because the irrigation systems were in place. Note the color-infrared print in Fig. 2a. The system on the north and east apparently includes a strip of actively growing vegetation. Region "A" is a seep caused by an excess of transported water either by overland flow or by lateral movement of groundwater.

Answers to specific questions of interest to the water resources or agricultural specialist were sought from the multistage, multispectral data. A visual interpretation of the films was conducted and results are in Table 5. Only the S192 high rate channels, which had DAS products available, and comparable aircraft spectral regions were evaluated.

A specific comparison includes fallow fields #7 and #13. Field #7 had been irrigated two days prior to the overflight and was wet at the very surface with no noticeable drying. Field #13 was dry. Notice that in the reflective spectral regions in Fig. 10 patterns occur within Field #7. These were associated both with normal soil variations and with variations caused by land leveling. Reflectance anomalies associated with soil moisture are not apparent between these two fields at wavelengths less than the 1.533→1.62 μm spectral channel.

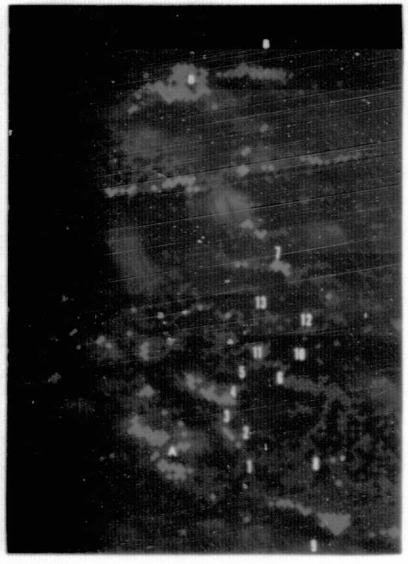

a. Channel 8, 0.68→0.76 μm

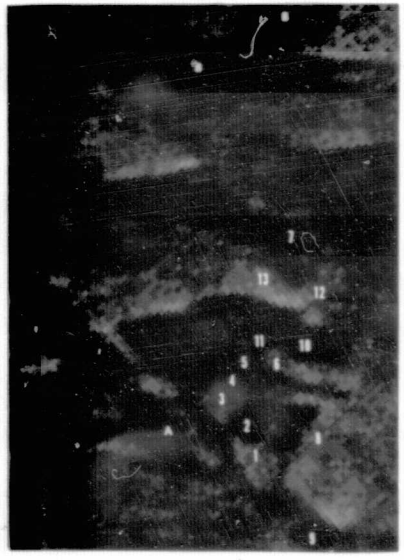

b. Channel 10, 0.78→0.88 μm

c. Channel 12, 1.55→1.75 μm

d. Channel 14, 2.10→2.35 μm

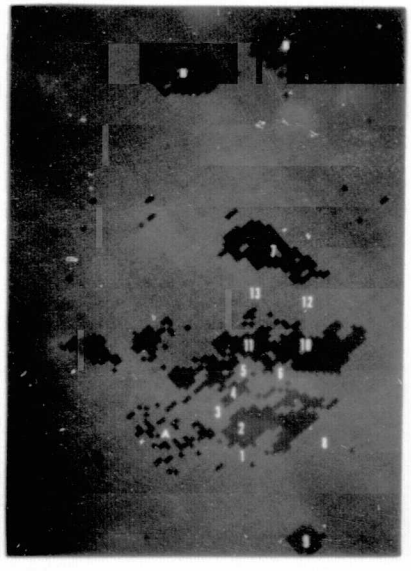

e. Channel 16, 10.2→12.5 μm

Fig. 9 - Photographic representations of the digital data acquired using the S192, multispectral scanner aboard SKYLAB. The conversion of the digital tapes to film was accomplished using the DAS system at JSC, Texas. Field numbers correspond to those in Fig. 2a and Table 1. A similar area as in Fig. 2a is included. Note the data from the conical scanner have not been rectified; therefore, the round pattern associated with the center pivots appears elliptical (original in color).

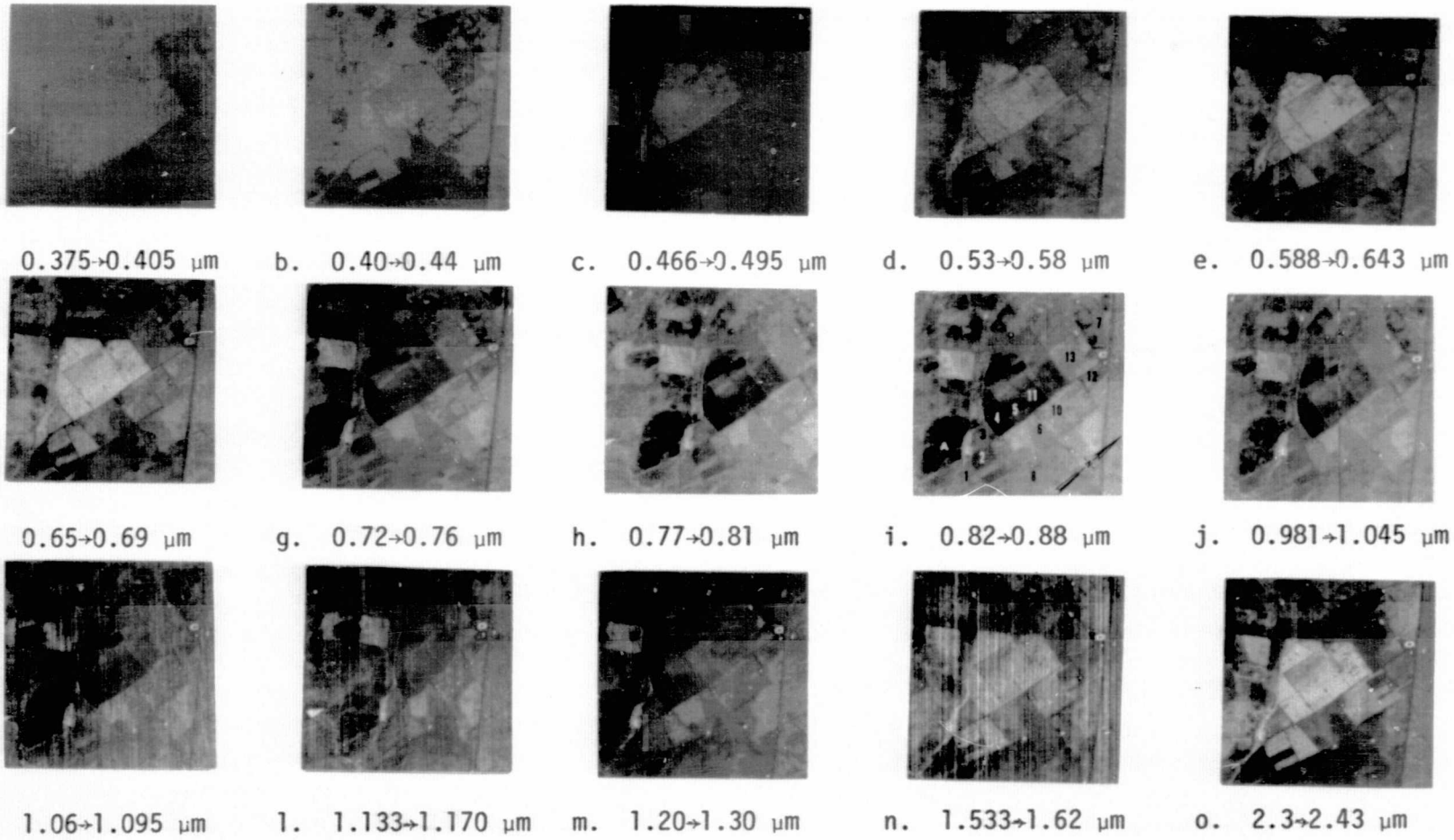

a. 0.375→0.405 μm b. 0.40→0.44 μm c. 0.466→0.495 μm d. 0.53→0.58 μm e. 0.588→0.643 μm

f. 0.65→0.69 μm g. 0.72→0.76 μm h. 0.77→0.81 μm i. 0.82→0.88 μm j. 0.981→1.045 μm

k. 1.06→1.095 μm l. 1.133→1.170 μm m. 1.20→1.30 μm n. 1.533→1.62 μm o. 2.3→2.43 μm

Fig. 10 - Photographic representations of the 24-channel multispectral scanner data acquired with the NASA, NC-130B aircraft at approximately 7620-m AGL (25,000 ft) on mission 258. The field numbers correspond to the field numbering in Fig. 2a and in Table 1. Dark is high reflectance in a → o and is warm for p → u. Field numbers are labeled in "i" and "t".

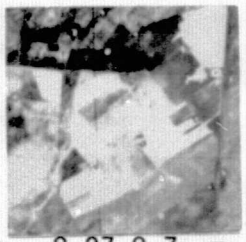

p. 8.27→8.7 μm

q. 8.8→9.3 μm

r. 9.38→9.876 μm

s. 10.1→11.0 μm

t. 11.0→12.0 μm

u. 12.0→13.0 μm

(Fig. 10 continued)

dark is warm, 10.2→12.5 μm

Fig. 11 - Thermal data from the NASA RB-57F aircraft mission 260 collected at 18,300-m AGL (60,000 ft) with the RS-7 scanner. Field numbers are the same as in Fig. 2a and Table 1. Approximate scale 1:50,000.

TABLE 5. RECOGNITION OF SELECTED LANDSCAPE FEATURES USING SKYLAB AND CORRESPONDING NC-130B DATA.

Landscape Feature	SKYLAB Data - wavelength in μm					Comparable NC-130B Data - wavelength in μm				
	0.68-0.76	0.78-0.88	1.55-1.75	2.10-2.35	10.2-12.5	0.70-0.76	0.82-0.88	1.533-1.62	2.3-2.43	11.0-12.0
Dry fallow vs. wet fallow (fields 6, 13 vs. 7,10)	no	no	yes	yes	yes	no	no	yes	yes	yes
"Well- or medium" watered vegetation vs. "wet" fallow (fields 4, 5 vs. 7, 10)	no	yes	no	no	no	yes	yes	no	no	no
"Well-watered" vs. "Dry" alfalfa (field 4 vs. 3)	no	yes	yes	yes	yes	yes	yes	yes	yes	yes
"Medium-watered" vs. "well-watered" alfalfa (field 5 vs. 4)	no	yes	no	no	yes	no	no	no	no	yes
Recognition of extent of seep (area A)	no	yes	yes	yes	yes	yes	yes	yes	yes	yes
Identification of center pivots (area B)	no	no	no	no	yes	NA 2/	NA	NA	NA	yes 3/
Survey of irrigated land	no	no	no	no	yes	no	no	no	no	yes
Unique location of surface water	no	no	yes	yes	no	yes	yes	yes	yes	no

1/ The observations are based on visual analyses of the original color DAS products and should be verified using statistical analyses of the digital data.

2/ Center pivots not imaged.

3/ Interpretation from the 10.2-12.5μm thermal scanner (RS-7) on RB-57F aircraft.

In the 1.533→1.62 μm and the 2.3 → 2.43 μm channels, a continuous pattern transecting the two fields appears to be related to soil variation other than soil moisture. The two fields are definitely contrasting in all the thermal bands. Field #10 is a fallow field which was under furrow irrigation at the time of the data collection. Again, wavelengths greater than 1.533→1.62 μm were effective for separating the wet versus dry fallow with no spectral differences apparent in the shorter reflective spectral regions. Similar spectral variations in the SKYLAB data are evident.

SKYLAB S193

No data.

SKYLAB S194

No analysis of data.

PRESENTATION OF STATISTICAL RESULTS

Classification of Fields Using Digitized S190-A Film

The correlations of the 30 separate field means for each of the S190-A films which were digitally analyzed are in Table 6. Each field mean was comprised of no less than 20 individual pixel observations. The mean values are presented in Table A-3 in Appendix A.

TABLE 6. CORRELATIONS OF SPECTRAL REGIONS OF THE S190-A FILMS.

	Spectral Region in μm			
	0.5→0.6	0.6→0.7	0.7→0.8	0.8→0.9
0.5→0.6	1.000			
0.6→0.7	0.869**	1.000		
0.7→0.8	-0.282	-0.346	1.000	
0.8→0.9	-0.448*	-0.567**	0.366*	1.000

where * is significant at the 0.05 level and ** is significant at the 0.01 level. 28df

The greatest redundancy among bands was between the 0.5→0.6 μm and the 0.6→0.7 μm bands which had an R^2 value of 75%. Other correlations

were significant but the coefficient of determination was small. A statistical classification of fields is presented in Table 7. For example, in Table 7 for the 0.7→0.8 μm region, ten classes of data were statistically separable at the 0.05 significance level for the 31 sites. Fields #4, 25, and 23 were separable from fields #5 and 11 from fields #22, 19, 24, 28, etc. No statistical separations among fields #4, 25, and 23 were present.

TABLE 7. RESULTS OF t-TEST USING THE MEAN SADE VALUE FOR FIELDS IN THE SKYLAB PROJECT. CLASSES ARE STATISTICALLY DIFFERENT FOR EACH SPECTRAL BAND USING A 0.05 CONFIDENCE LEVEL. THE FIELD NUMBERS CORRESPOND TO THOSE IN FIG. 2 AND TABLE 1.

Class number	0.7→0.8 μm Station A-1 Field(s)	0.8→0.9 μm Station A-2 Field(s)	0.6→0.7 μm Station A-5 Field(s)	0.5→0.6 μm Station A-6 Field(s)
1	4,25,23	4,5,21	23	8
2	5,11	11	8	23,1
3	22,19,24,28	17,30,18,15, 22,8,3,1,2	1,15	22,13,12,16
4	2,3,1,18,8, 21	13,24,31,19, 20,23,10,12, 7,29,25	16,28,22,14 17,21,13,12	7,10,15,14, 2,29
5	29,30	28,26,6	31,10,25,27, 7,29,26,2	27,21,6,19, 26,28
6	20,13,12,10, 27,16,14	16,27	6	17,30,25,3, 18,31,24,20
7	7,15,6,26	14	30,19,20,24	4,11
8	31	9	3	5
9	17	-	18	9
10	9	-	4,5,11,9	-

The relationship of spectral data to ground information is presented using correlation coefficients in Table 8. The 0.6→0.7 μm spectral

band accounted for the greatest amount of variation (36%) in the 0→2 cm soil moisture measurements. A significant correlation with the 2→10 cm soil moisture was also obtained in the 0.6→0.7 μm region; however, note from Table 4 that the two depths of soil moisture were highly correlated. Therefore, a correlation with one variable implies a correlation with the second. The same is the case for correlation with the composite moisture because the composite moisture is composed of the individual soil layers combined. The 0.7→0.8 μm region provided highly significant correlations with variations of percent green vegetation and percent fallow soil. The 0.6→0.7 μm region of the S190-A sensor would be used for soil moisture predictions with the 0.7→0.8 μm band for estimates of land cover if only these data were available.

TABLE 8. CORRELATION OF S190-A TO GROUND VARIABLES.

	Spectral Region in μm			
	0.5→0.6	0.6→0.7	0.7→0.8	0.8→0.9
Soil moisture				
0 → 2cm	0.404*	0.598**	-0.322	-0.411*
2 → 10cm	0.222	0.371*	-0.166	-0.127
10 → 30cm	0.258	0.296	-0.142	-0.047
Composite	0.279	0.368*	-0.177	-0.115
Land Use				
% green vegetation	0.565**	0.561**	-0.675**	-0.367*
% dry debris	-0.233	-0.058	-0.073	0.039
% fallow	-0.324	-0.440*	0.628**	0.287

where * is significant at the 0.05 level and ** is significant at the 0.01 level. 28df

Effect of Look Angle and Atmospheric Path Length on S191-measured Radiance

Calibrated radiance values from a range of look angles from 45° forward to 0° were computed. Radiance values within each equivalent S192 wavelength interval were averaged. Radiance versus atmospheric path length was evaluated. The atmospheric path length at 0° look

angle was assumed to be of zero distance because the actual atmospheric layering of the various absorbing and scattering constituents was unknown. At a 45° look angle for the SKYLAB altitude, the relative increase in path length from the sensor to the land surface was 149 km when compared to the distance at nadir. Therefore, the regression of changing scene radiance, which was computed using the S191 sensor as the dependent variable and changing path length as the independent variable from 0→149 km, should be linear with respect to atmospheric thickness of the various constituents. Sensor-measured radiance changes with differing look angles are not only a function of atmospheric path length but are also a function of sensor-to-target-to-sun angles for the reflecting scene. Therefore, the regressions include both variance associated with atmospheric thickness and geometry. Assuming the presence of a Rayleigh atmosphere which had minimal scattering in the longer reflective infrared wavelengths and that the geometry variations were not wavelength dependent allowed partitioning of the atmospheric and geometric variance by subtraction of the slope of the regression for the longer wavelengths (the value of 4.5×10^{-7} for 2.12→2.36 μm range) from the slope of the shorter wavebands (see Table 9). If these assumptions hold, the remaining value is attributed to the atmospheric component.

The regressions were significantly different than $b_0=0$ at the 0.01 level for all wavebands evaluated. The positive slopes for the reflective regions or the increasing S191-measured radiance with increasing path length indicate the influence of the atmospheric scattering. The negative slope of the thermal band reveals the cooling effect of the atmosphere when the effective atmosphere is cooler than the radiating surface. Relative atmospheric radiation was 44 times greater in the 0.41→0.46 μm spectral region than in the 1.56 →1.74 μm spectral region. Regression coefficients progressively were larger from the longer reflective-infrared wavelengths to the shorter wavelengths in the visible spectrum except in the water absorption region of 1.10→1.18 μm where absorption probably reduced the measured scattering effect.

Classification of Fields Using S192 Data

The correlation among spectral regions of the S192 scanner using paired observations of the means from each of the 30 separate fields

TABLE 9. REGRESSION COEFFICIENTS OF THE S191 SENSOR TO ATMOSPHERIC THICKNESS AND SENSOR GEOMETRY FOR THE S192 SPECTRAL REGIONS.

Spectral band in μm	Slope of Regression As Function of both Atmosphere and Geometry (b) 1/	Slope of Regression As Function of Atmosphere (b-0.045) 1/	Relative Atmospheric Radiation $\left(\frac{b-0.045}{0.084}\right)$
0.41 → 0.46	3.721**	3.676	43.8
0.46 → 0.51	3.283**	3.238	38.5
0.52 → 0.55	2.903**	2.858	34.0
0.56 → 0.61	2.340**	2.295	27.3
0.62 → 0.67	2.235**	2.190	26.1
0.68 → 0.76	2.200**	2.155	25.6
0.78 → 0.88	1.995**	1.950	23.2
0.98 → 1.08	0.967**	0.922	10.9
1.10 → 1.18	0.428**	0.383	4.5
1.20 → 1.74	0.498**	0.453	5.4
1.56 → 1.74	0.129**	0.084	1.0
2.12 → 2.36	0.045**	0.000	
10.2 → 12.2	-0.029**		

where * is for b significantly different than b =0 at the 0.05 level and ** at the 0.01 level, b is the slope of the regression line, Y is the dependent variable (S191-measured radiance), and X is the independent variable (relative atmospheric path length).

1/ all exponents are 10^{-5}

are in Table 10. The mean radiance value by spectral region for each field is in Table A-4 in Appendix A. Few correlations among various spectral regions were significant. The thermal channel of 10.2→12.5 μm and reflective infrared 2.1→2.35 μm channel had a coefficient of determination of 75%. Visual interpretation of the scanner products revealed that both of these channels varied with water-related terrain features and would, therefore, probably be correlated with each other. Most of the reflective-infrared channels were not significantly correlated.

A statistical classification of fields based upon the S192 channels is presented in Table 11. Field groupings within each of the spectral bands were significantly different at the 0.05 level using the two-tailed t-test. The relationship of the classification to ground data is presented using correlation coefficients in Table 12.

Percent dry debris was significantly correlated with the 1.55→1.75 μm spectral region. The surface 0→2 cm moisture was correlated with the two reflective-infrared channels which had wavelengths longer than 1.55 μm and with the thermal-infrared channel. The near-surface soil moisture data of 2→10 cm and the composite soil moisture data were significantly correlated with the 1.55→1.75 μm spectral region. The thermal region significantly correlated with the 10→30 cm and composite soil moistures. Therefore, to prepare an enhancement map illustrating soil moisture variations using the field groups (with associated means and standard errors) presented in Table 11, either the groupings for the 1.55→1.75 μm or 10.2→12.5 μm spectral region should be included.

The thirty individual fields were stratified into crop, fallow, and range for further correlation analyses. The range category contained only three fields and that category was dropped. Fallow and cropped categories were separated by percent vegetation with the requirement of greater than 20% green vegetation for the cropped category. Fourteen fields were classified as cropped and 13 as fallow. The correlation of spectral data from the S192 sensor to ground variables for the cropped and fallow categories are in Table 13. In general, the correlations between ground variables and spectral regions for the fallow fields were greater than for the cropped fields. For the fallow fields, the thermal-infrared region was consistently correlated with soil moisture.

TABLE 10. CORRELATION OF SPECTRAL REGIONS OF THE S192 SKYLAB SCANNER USING THE 30 SEPARATE FIELDS AS OBSERVATIONS.

Channel (s)		Spectral region in μm							
		0.56→ 0.61	0.68→ 0.76	0.78→ 0.88	0.98→ 1.08	1.09→ 1.19	1.55→ 1.75	2.1→ 2.35	10.2→ 12.5
3-4	0.56→0.61	1.000							
7-8	0.68→0.76	0.227	1.000						
9-10	0.78→0.88	-0.155	0.712**	1.000					
19	0.98→1.08	-0.378*	-0.002	-0.090	1.000				
20	1.09→1.19	0.020	-0.176	-0.329	0.006	1.000			
12	1.55→1.75	0.139	-0.273	-0.495**	-0.151	-0.129	1.000		
13-14	2.1→2.35	0.868**	0.115	-0.245	-0.270	0.085	0.093	1.000	
15-16	10.2→12.5	0.630**	0.010	-0.240	-0.090	0.077	0.027	0.869**	1.000

where * is significant at the 0.05 level and ** is significant at the 0.01 level. 28df

TABLE 11. RESULTS OF THE t-TEST USING MEAN RADIANCE VALUES FOR FIELDS FROM THE S192 DATA. CLASSES ARE STATISTICALLY DIFFERENT FOR EACH SPECTRAL BAND USING A 0.05 CONFIDENCE LEVEL.

Class Number	0.56→0.61μm Channel 3-4 Field(s)	0.68→0.76μm Channel 7-8 Field(s)	0.78→0.88μm Channel 9-10 Field(s)	0.98→1.08μm Channel 19 Field(s)	1.09→1.19μm Channel 20 Field(s)	1.55→1.75μm Channel 12 Field(s)	2.1→2.35μm Channel 13-14 Field(s)	10.2→12.5μm Channel 15-16 Field(s)
1	28,30,13,12, 29, 1,20,16, 27,19, 7, 8, 24,26	25,30,17,29, 16	25,21,17,14, 23,30,29,16, 19,26	18	4,16,19, 8, 26,22,20, 3	13,29,24,12, 16	13,28	28,13,31,16, 12,29,27,30, 8, 3
2	31,25, 2,17	4,23, 8,26, 19,28,20,31, 1, 3,21,14	31,20,28, 3, 22, 8, 6,27, 7, 2,11,10, 4,15, 5,12, 9,13,18	4	1	1,17,19,25, 22, 8,30,26, 3,15	12,16,30,20, 29,26	15,20,26, 1
3	10, 5,15,11, 3,22, 6	22, 7,27,11, 15,12, 5, 2, 13	-	17,26,29,22, 8,27,16,19, 14	11	6,27, 5,31, 20, 7,11	27	24,19, 5,18, 6
4	14,23	6,10,18	1	1,20, 3,15 2, 7,11,23 5,31,30	18,25,17,15, 12, 5,30, 7,	28,10, 2, 4, 23,21	1,31,24,19 8	22,14,25
5	4	24	24	6,12,10,13	23,14,31,21, 2,27,13,11, 10, 6	14	15, 6	4,17,23,11, 21,2
6	18,21	9	-	25,24,21,28	28,24	18	3,25,22,17, 5	7,10
7	9	-	-	9	9	9	11	9
8	-	-	-	-	-	-	7,18,10,14, 2	-
9	-	-	-	-	-	-	23, 4	-
10	-	-	-	-	-	-	21	-
11	-	-	-	-	-	-	9	-

TABLE 12. CORRELATION OF S192 DATA TO GROUND DATA FOR 30 TEST FIELDS.

	Spectral Region in μm							
	0.56→ 0.61	0.68→ 0.76	0.78→ 0.88	0.98→ 1.08	1.09→ 1.19	1.55→ 1.75	2.1→ 2.35	10.2→ 12.5
Soil moisture								
0 → 2cm	-0.116	-0.251	-0.360	-0.034	0.193	0.455*	-0.366*	-0.479**
2 → 10cm	0.124	-0.234	-0.326	-0.205	0.103	0.533**	-0.104	-0.340
10 → 30cm	-0.091	-0.123	-0.133	-0.283	0.064	0.282	-0.112	-0.419*
Composite	0.075	-0.175	-0.219	-0.247	0.093	0.386*	-0.145	-0.426*
Land Use								
% green vegetation	-0.359	-0.033	-0.031	0.167	0.078	-0.119	-0.342	-0.248
% dry debris	0.203	0.226	-0.138	0.009	0.079	0.386*	0.215	0.277
% fallow	0.168	-0.127	0.121	-0.149	-0.121	-0.162	0.145	0.023

where * is significant at the 0.05 level and ** is significant at the 0.01 level. 28df

TABLE 13. CORRELATION OF S192 DATA TO GROUND VARIABLES FOR THE 14 CROPPED AND 13 FALLOW FIELDS.

	Spectral Region in μm							
	0.56→0.61	0.68→0.76	0.78→0.88	0.98→1.08	1.09→1.19	1.55→1.75	2.1→2.35	10.2→12.5
Cropped (12df)								
Soil Moisture								
0 → 2cm	-0.259	-0.156	-0.488	0.030	0.296	0.495	-0.250	-0.347
2 → 10cm	0.186	-0.026	-0.369	-0.307	0.316	0.522	0.102	-0.131
10 → 30cm	0.303	0.212	-0.061	-0.420	0.244	-0.036	0.120	-0.233
Composite	0.216	0.113	-0.210	-0.361	0.292	0.186	0.072	-0.243
Land Use								
% Green Vegetation	-0.426	0.018	-0.067	0.288	-0.117	-0.208	-0.375	-0.505
Fallow (11df)								
Soil Moisture								
0 → 2cm	0.104	-0.334	-0.242	-0.212	-0.225	0.492	-0.358	-0.688**
2 → 10cm	0.292	-0.329	-0.387	-0.183	-0.185	0.613*	-0.068	-0.686**
10 → 30cm	0.127	-0.319	-0.271	-0.237	-0.207	0.542	-0.103	-0.681*
Composite	0.177	-0.333	-0.310	-0.226	-0.209	0.574*	-0.123	-0.704**

where * is significant at the 0.05 level and ** is significant at the 0.01 level.

Enhancement of S192 Digital Data by Statistical Techniques

Many man-machine interactive procedures allow the interpreter to level slice the original digital data to enhance certain scene contrasts which are related to specific thematic interpretations. Equal level slicing was presented in the example DAS products in Fig. 9. The procedure developed for enhancing the S192 data was to base the levels for slicing on the statistical classification presented in Table 11 and to use unequal levels for slicing. The class means were compared with weighting between means based upon the standard deviations of the adjacent means. This procedure was used to develop separation levels for a variable quantizer program to level slice the digital data and to display the data on a color screen via SADE. The ground region is similar to that for the DAS products in Fig. 9 and the photography in Fig. 2a, both of which included ground sites #1→13. The color enhanced products are presented for the six different high-rate channels in Fig. 12. Since the channel 11 data were not of sufficient quality for use, the pixels within a line of data from channel 12 were doubled to retain similar geometry as in the other five channels. The DAS product for the 10.2→12.5 μm presented in Fig. 9 had two separate levels; whereas, the data in the thermal channel presented in Fig. 12 has five separate levels (levels determined using statistical t-test classification of sites #1→13). Based upon the correlation results of these channels to the ground variables for the 30 test fields, the ground variables most related to the spectral data were: 0.56→0.61 μm for percent green vegetation ($r = -0.359$), 0.68→0.76 μm for 0→2 cm soil moisture ($r = -0.251$), 0.78→0.88 μm for 0→2 cm soil moisture ($r = -0.360$), 1.55→1.75 μm for 2→10 cm soil moisture ($r = 0.533^{**}$), 2.1→2.35 μm for 0→2 cm soil moisture ($r = -0.366^{*}$), and 10.2→12.5 μm for 0→2 cm soil moisture ($r = -0.479^{**}$).

Recognition of Water-Related Terrain Features from S190-A and S192 Statistical Classification

The same resource questions were asked of the statistical classification of data as were asked of the visual interpretation presented in Table 5. The results in Table 14 are based upon observations from the same fields as the visual evaluation with the assumption that the

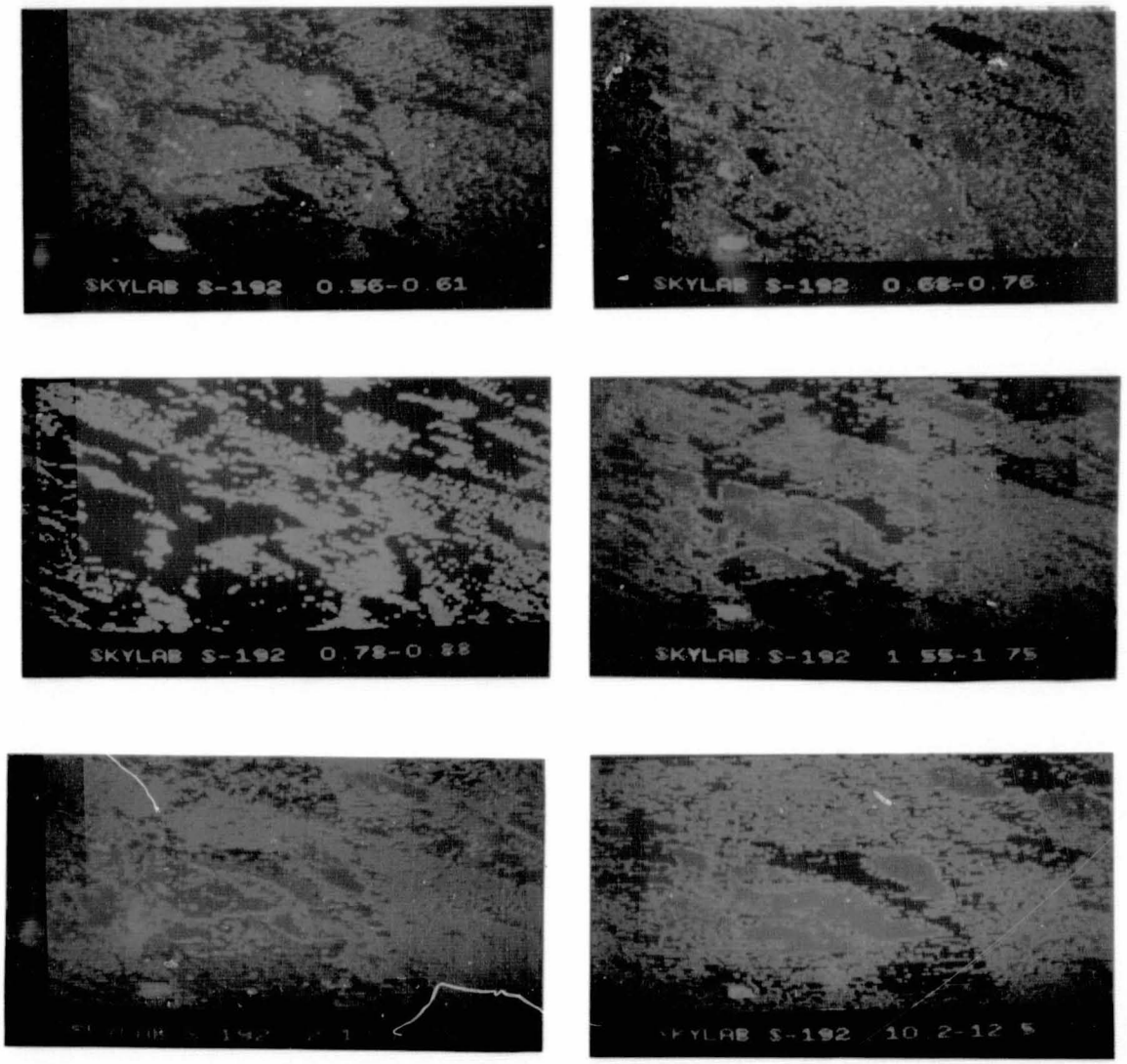

Fig. 12 - Color-enhanced products of the high-rate S192 channels. Levels chosen based upon statistical separation of the fields (original in color).

TABLE 14. RECOGNITION OF SELECTED LANDSCAPE FEATURES USING S192 AND S190-A DATA AND THE t-TEST RESULTS OF SCENE CLASSIFICATION AT THE 0.05 SIGNIFICANCE LEVEL INCLUDING COMPARISON OF NC-130B AIRCRAFT SCANNER.*

LANDSCAPE FEATURE	S192 SPECTRAL REGION IN μM								S190-A SPECTRAL REGION IN μM			
	0.56→0.61	0.68→0.76	0.78→0.88	0.98→1.08	1.09→1.19	1.55→1.75	2.1→2.35	10.2→12.5	0.5→0.6	0.6→0.7	0.7→0.8	0.8→0.9
Dry fallow vs. wet fallow (6,13 vs 7,10)	no(no)***	no(no)	no(no)	no(no)	no	no(no)	yes(yes)	yes(yes)	no	no	no	no
"well- or medium-" watered vegetation vs. wet fallow (4,5 vs 7,10)	no(yes)	no(yes)	no(yes)	no(yes)	no	no(no)	no(yes)	yes(yes)	yes	yes	yes	yes
well-watered vs. "dry" alfalfa (4 vs 3)	yes(yes)	no(yes)	no(yes)	yes(yes)	no	yes(yes)	yes(yes)	yes(yes)	yes	yes	yes	yes
medium-watered vs. well-watered alfalfa (5 vs 4)	yes(yes)	yes(yes)	no(yes)	yes(yes)	yes	yes(no)	yes(no)	yes(yes)	yes	no	yes	no
Survey of Irrigated** Land	no(no)	no(no)	no(no)	no(no)	no	no(no)	no(no)	yes(yes)	no	no	no	no
Unique location of Surface water	yes	yes	no	yes	yes	yes	yes	yes	yes	no	yes	yes

* The statistical classes must be separable and when more than one field is included, the fields must rank in similar order to obtain a yes answer.
** All preceding answers must be positive before entering a yes.
*** Closest corresponding NC-130B scanner digital interpretation (0.54→0.58, 0.71→0.76, 0.83→0.88, 0.98→1.04, 1.53→1.63, 2.1→2.38, and 11.2→11.9 μm respectively.

fields were representative of the area analyzed. Alfalfa fields with similar canopies and varying soil moisture levels were used for interpretation of irrigation scheduling. Results similar to those in Table 5 were obtained for the discrimination between wet and dry fallow surfaces, that is, only the longer reflective-infrared wavelengths and the thermal infrared data were effective for spectral recognition. The only data which could be effectively used for a survey of irrigated lands were in the thermal spectral band. An analysis of corresponding scanner data from the NC-130B aircraft is included in Table 14. The statistical field classification for the 12 test fields (those in Fig. 2a) is presented in Table A-5 of Appendix A. Many additional water-related features were separable in the NC-130B data that were not separable in the SKYLAB data, especially in the shorter wavelength regions. However, the survey of irrigated land could only be conducted with the thermal data for both the NC-130B and SKYLAB data. The criteria for a yes answer to this question was for all preceding categories to have a yes answer (Table 14).

Least-Squares Multiple Regression for Prediction of Ground Variables

An advantage of a multispectral scanner is the automatic registration of data from various spectral regions. Therefore, the combined use of spectral qualities can be easily attained for prediction of a dependent variable from a combination of independent variables of spectral data. The field means of spectral information from the spectral regions of the S192 scanner were used to predict the soil moisture variables. Eight spectral regions of the S192 were considered as independent variables. The computer program used for the analysis chose, as the first independent variable, the input which accounted for the greatest reduction in error sum of squares. The second variable was automatically chosen which, when in combination with the first selected variable, provided the greatest additional reduction in error sum of squares. This procedure continued until the error sum of squares was either zero valued or until all possible independent variables had been selected. The F-test in an analysis of variance was then used to determine which independent variables should be included in the equation at a given level of significance. The multiple correlation coefficient (R) and coefficient of determination (R^2) were also program outputs. An example analysis is illustrated

in Table 15 for prediction of the composite soil moisture. A summary of multiple regression analyses for all 30 fields, the 14 cropped fields, and the 13 fallow fields is in Table 16. Only those independent variables which were significant at least at the 0.05 confidence interval were included in the equation.

The resulting equation from Table 15 for predicting the composite soil soil moisture is:

$$y = -10.8\ x_1 - 1.7\ x_2 + 0.6\ x_3 + 111.9 \qquad [17]$$

where y = composite soil moisture

x_1 = radiance from 10.2→12.5 μm region

x_2 = radiance from 0.98→1.08 μm region

x_3 = radiance from 1.55→1.75 μm region

The coefficient of determination (R^2) for this equation for the thirty observations was 52.4%.

Equations were developed which accounted for 46→54% of the variation in soil moisture with spectral data when both cropped and fallow fields were included in the analysis. The 10.2→12.5 μm, 1.55→1.75 μm, and 0.98→1.08 μm spectral regions were the predominant independent variables chosen. For the cropped fields alone, no variables alone (note Table 12) or in combination yielded an equation which was significantly related to soil moisture. The spectral regions of 10.2→12.5 μm, 1.55→1.75 μm, and 0.56→0.61 μm were chosen in that order for prediction of each of the soil moisture variables except for the 10→30 cm depth where only the first two were chosen. Coefficients of determination ranged from 71→90%. Since no significant equations could be developed for the cropped fields and the equations developed for the fallow fields had larger correlation coefficients, the fallow fields probably had a considerable influence on the significance of the equations developed for all fields.

The relationship of the predicted versus actual composite soil moisture values using the regression equations is in Fig. 13. The actual composite soil moisture was plotted against the predicted soil moisture for the fallow fields in Fig. 13a and for all fields in Fig. 13b. The actual regressions could not be plotted because three independent variables were included in each equation. However, Fig. 13 displays the variance in prediction.

TABLE 15. EXAMPLE ANALYSIS OF VARIANCE OF MULTIPLE REGRESSION FOR PREDICTING THE COMPOSITE SOIL MOISTURE WITH S192 DATA FOR ALL FIELDS.

Dependent Variable -- Composite Soil Moisture

Independent Variable Radiance from Given S192 Spectral Region in μm	Sum of Squares	Degrees of Freedom	Mean Square	F-Value	R	R^2(100) in Percent
10.2→12.5	143.62	1	143.62	11.7**		18.9
0.98→1.08	164.83	1	164.83	13.5**		40.7
1.55→1.75	89.19	1	89.19	7.28*	0.724**	52.4
1.09→1.19	34.62	1	34.62	2.8		57.0
0.68→0.76	28.74	1	28.74	2.3		60.7
0.56→0.61	13.93	1	13.93	1.1		62.6
2.1→2.35	25.93	1	25.93	2.1		65.9
0.78→0.88	0.79	1	0.79	0.1		65.9
Error	257.29	21	12.25			
Total	758.94	29				

where * is significant at the 0.05 level and ** is significant at the 0.01 level.

TABLE 16. SUMMARY OF MULTIPLE REGRESSION ANALYSES FOR PREDICTION OF SOIL MOISTURE CONTENTS USING THE S192 DATA. ONLY VARIABLES SIGNIFICANT AT LEAST AT THE 0.05 LEVEL ARE INCLUDED IN EQUATIONS.

Land Use	Number of Fields	Dependent Variable (Soil Moisture)	Independent Variables						R[3]	(R^2)[4]
			b_1[1]	x_1[2]	b_2	x_2	b_3	x_3		
No Stratification	30	0 → 2cm	-17.4	10.2→12.5	-2.0	0.78→0.88			0.684	46.8%
		2 → 10cm	0.9	1.55→1.75	-9.5	10.2→12.5	-1.3	0.98→1.08	0.737	54.4%
		10 → 30cm	-10.9	10.2→12.5	-2.0	0.98→1.08			0.659	43.4%
		Composite	-10.8	10.2→12.5	-1.7	0.98→1.08	0.6	1.55→1.75	0.724	52.4%
Cropped	14	0 → 2cm	none significant							
		2 → 10cm	none significant							
		10 → 30cm	none significant							
		Composite	none significant							
Fallow	13	0 → 2cm	-23.0	10.2→12.5	1.3	1.55→1.75	5.2	0.56→0.61	0.921	84.8%
		2 → 10cm	-16.9	10.2→12.5	1.0	1.55→1.75	2.0	0.56→0.61	0.947	89.7%
		10 → 30cm	-13.5	10.2→12.5	0.9	1.55→1.75			0.848	71.8%
		Composite	-15.6	10.2→12.5	0.9	1.55→1.75	1.2	0.56→0.61	0.906	82.1%

1/ where $b_1, b_2, \ldots b_n$ are the partial regression coefficients,

2/ where $x_1, x_2, \ldots x_n$ are the independent variables,

3/ where R is the multiple correlation coefficient of resulting equation, and

4/ where R is the coefficient of determination of the resulting equation. The equation form is $y = b_1x_1 + b_2x_2 + \ldots\ldots b_nx_n + c$

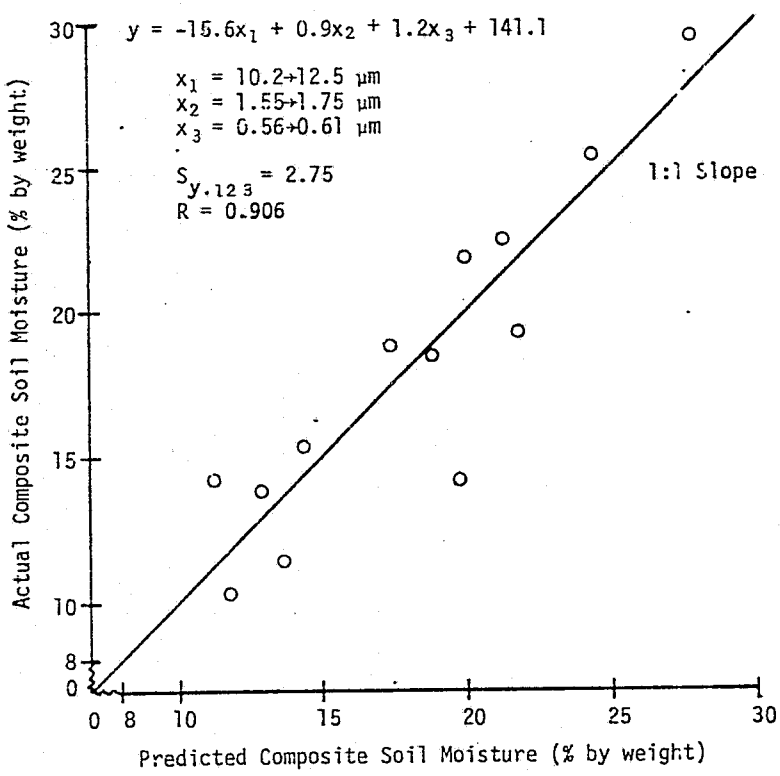

a. Fallow Fields - 13 Fields

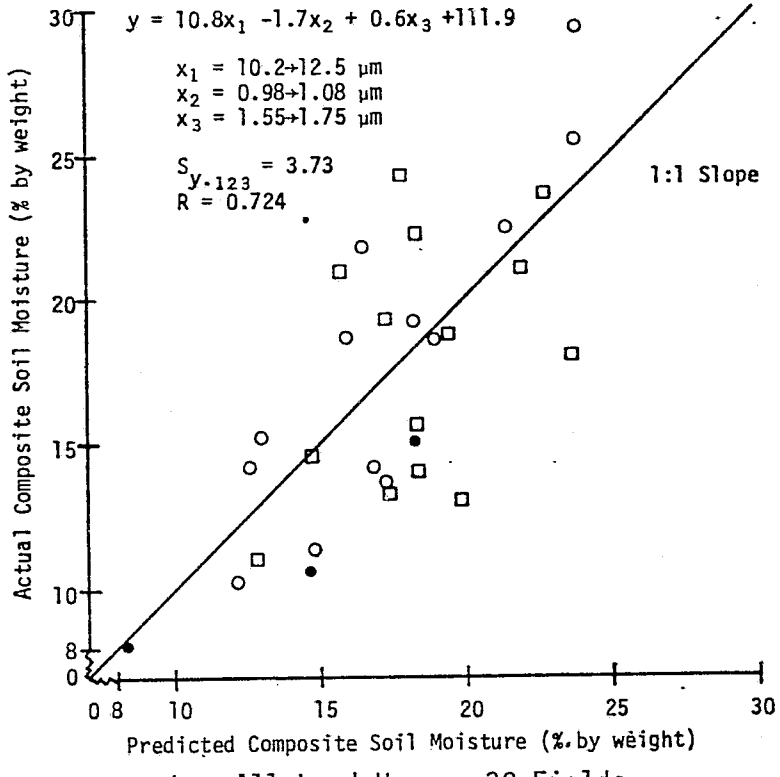

b. All Land Uses - 30 Fields

Figure 13 - Predicted versus actual composite soil moisture (0→30 cm) for the test fields using the multiple regression equations with S192 data as independent variables. The "○" denotes fallow, "•" denotes range, and "□" denotes cropped surfaces.

SOIL THERMAL PROPERTY AND EVAPOTRANSPIRATION ASSESSMENTS

Preparation of Evapotranspiration Map

The Jensen-Haise model was used for an estimate of ET, where:

$$ET_p = (0.025\ T + 0.08)\ R_s \qquad [9]$$

where ET_p = potential ET in mm min^{-1}

T = air temperature in degrees C

R_s = equivalent depth of evaporation of incoming solar radiation in mm min^{-1}.

Incoming solar radiation at the SKYLAB overpass (20:12 GMT) was measured with an Eppley pyranometer as 1.020 cal cm^{-2} min^{-1} with the air temperature as 19.3 C. Therefore, the potential ET prediction is 10.0 x 10^{-3}mm min^{-1}. Assume that: 1) the actual ET is equal to the potential ET for the field having the coolest surface temperature, 2) the actual ET is zero for the field with the warmest temperature, and 3) the temperature in the Jensen-Haise model is linearly related to the fourth root of the radiance as measured by the S192 scanner. The data set was used which covered a similar area as presented in Fig. 2a. Therefore, the 13 representative field sites in this region were statistically classified using the 10.2→12.5 μm channel. The field groupings were: Class I = #13, 2; Class II = #8, 3, 1; Class III = #5, 6: Class IV = #4, 11, 2, 7, 10; and Class V = #9. Corresponding class means and standard errors of the means were computed with subsequent groupings of the S192 digital data into the variable quantizer program. The Class V data corresponded to field #9 which was a free-water surface. The Class IV fields were assumed to have actual ET at the potential ET rate as predicted using the Jensen-Haise model (10.0 x 10^{-3} mm min^{-1}). Since the data were acquired under low ET demands and the Class IV fields represented high soil moisture regions with water freely available for evaporation and transpiration, this assumption was probably valid. The Class I fields of #13 and 12 were dry fallow and alfalfa, respectively, which had considerable soil water deficits. The ET was, therefore, assumed to be 0 mm min^{-1}. The Class I fields corresponded to the maximum class temperature with the Class IV fields corresponding to minimum class temperature of the agricultural fields. The remaining two classes were weighted using the fourth root of thermal radiance

and had calculated ET values of 8.4×10^{-3}mm min^{-1} and 5.4×10^{-3} mm min^{-1}. The resultant ET map is presented in Fig. 14. This procedure was developed to suggest alternative methods for deriving a coefficient similar to the crop coefficient which can be used to relate actual ET to potential ET. The synoptic, yet detailed, observations from satellite altitudes coupled with ET estimates can be useful in irrigation scheduling, watershed water budget models, monitoring crop growth and yields, etc. A multiple regression prediction using more than one spectral region may provide improved estimates since an improved relationship to actual soil moisture values for the reported observations was attained for equations developed using this technique.

Prediction of Soil Thermal Properties

The heat capacities of soils can be derived by summing the heat capacities of individual soil constituents per unit volume. DeVries (1963) reported that the heat capacity relationship to soil constituents could be summarized by:

$$c = 0.46\ x_1 + 0.60\ x_2 + x_3 \qquad [18]$$

where c = heat capacity in cal cm^{-3} C^{-1}, x_1 = volume fraction of soil minerals, x_2 = volume fraction of soil organic matter, and x_3 = volume fraction of soil water.

A typical volume fraction of soil minerals is 50% and a 4% volume fraction of soil organic matter. The volume fractions for a given soil do not change appreciably with time; however, the water content does change. Therefore, the prediction of changing soil moisture levels can be used to predict the changes in soil heat capacity. For fallow fields, a predictive soil moisture regression equation using S192 data had a multiple correlation coefficient of 0.906. If the soil bulk density and organic matter remain constant, the same correlation coefficients apply for the relationship of S192 data to soil heat capacity under fallow conditions. Water also has a considerable influence on the thermal conductivity of soils (the resistance of a soil to the transfer of heat). Therefore, the prediction of soil moisture from remotely sensed data provides an estimate of both heat capacity and thermal conductivity.

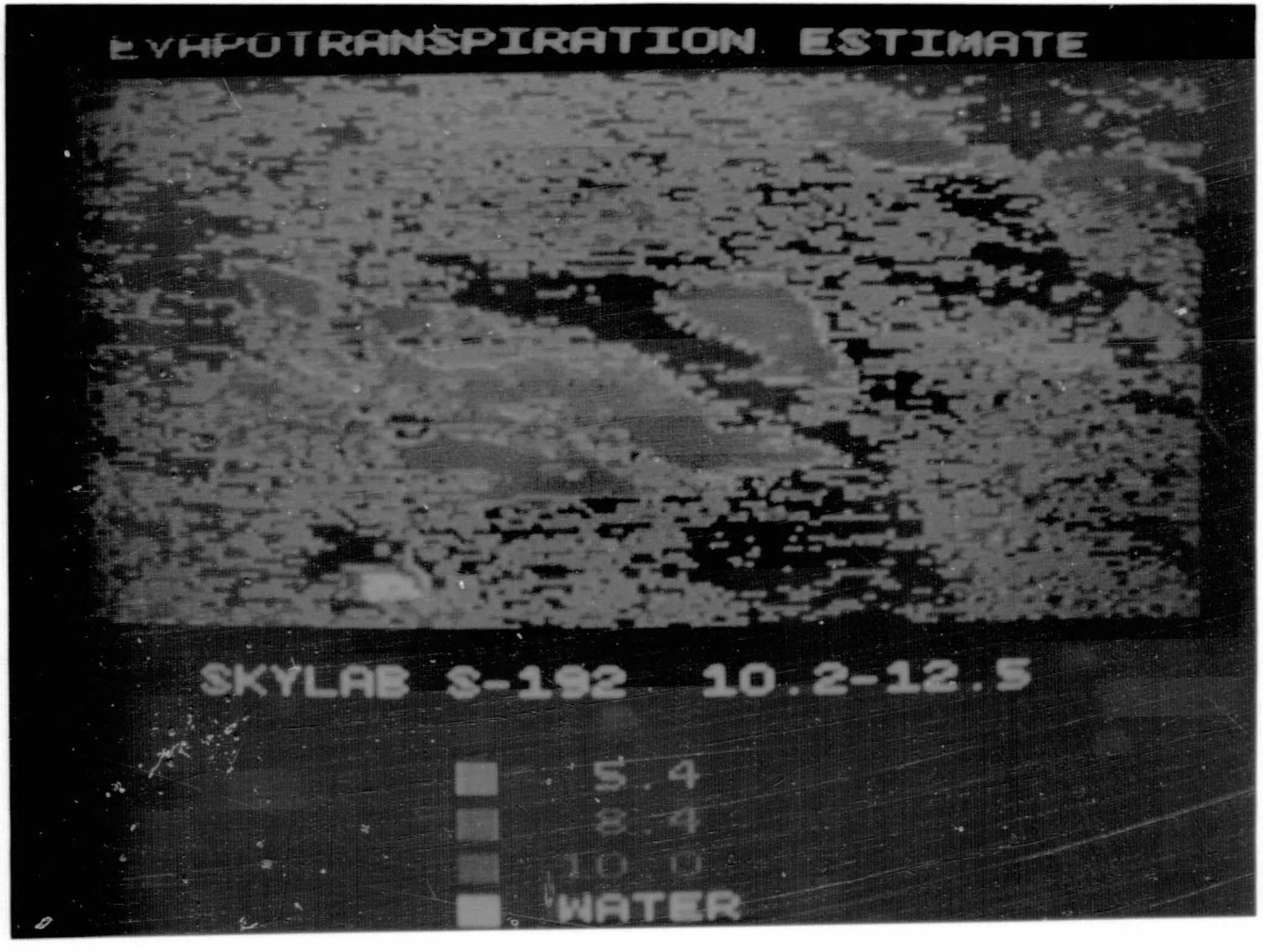

Fig. 14 - Evapotranspiration assessment of intensive test site prepared using thermal radiance estimates from the S192 scanner as an input into the Jensen-Haise equation (original in color).

Timing of Thermal Data Collection

The equivalent blackbody surface temperatures of fallow soils under wet and dry conditions are shown in Fig. 15 for one diurnal cycle. The wet and dry fields represented are #7 and 13, respectively -- refer to Fig. 2a. The precision radiation thermometer (PRT) temperature differential between the wet and dry surfaces at 14:12 CST was approximately 6 C, well within the thermal resolution of the X/5 S-192 SKYLAB detector. Prior to 9:00 CST and after 18:00 CST, the two fields could not be separated by surface emittance measurements which emphasizes the importance of the time of data collection in surface temperature observations. Note that during predawn hours, only a negligible temperature anomaly is present. If the energy budget differences were only conductive between the two fields, temperature differences should have been noted during predawn hours. Daytime heating of fallow soil surfaces can serve to indicate a deficit in the supply of water to the evaporating surface. Cool evaporating surfaces in an otherwise moisture deficient area indicate high soil moisture regions.

Survey of Irrigated Land With Remote-Sensor Data

An advantage of remote sensing is the synoptic view which allows data collection over large areas in a small time period. For the South Texas region in the low rainfall month of January, normally the only high soil moisture fields are those which have been recently irrigated. One approach to a survey of irrigated lands in this region of low rainfall is to identify all fields which have been converted from rangeland to cropland. Since most of the intensive agriculture in this region must be irrigated, a survey can be based upon recognition of the geometric patterns associated with fields. A survey such as this can be conducted with data such as the high-altitude aircraft photography presented in Fig. 2 or such as the space-altitude photography in Fig. 1. However, many of the fields have very low soil moisture because of the seasonal changes in land use and crop growth. A survey of irrigated lands using the pattern interpretation of the photographic data would, during many seasons, considerably overestimate the land actually under irrigation at a point in time. Since the thermal data from both the aircraft and SKYLAB altitudes could be effectively used to survey soil moisture variations, a survey of irrigated lands can be effectively accomplished using this spectral region. An example map of the irrigated lands of

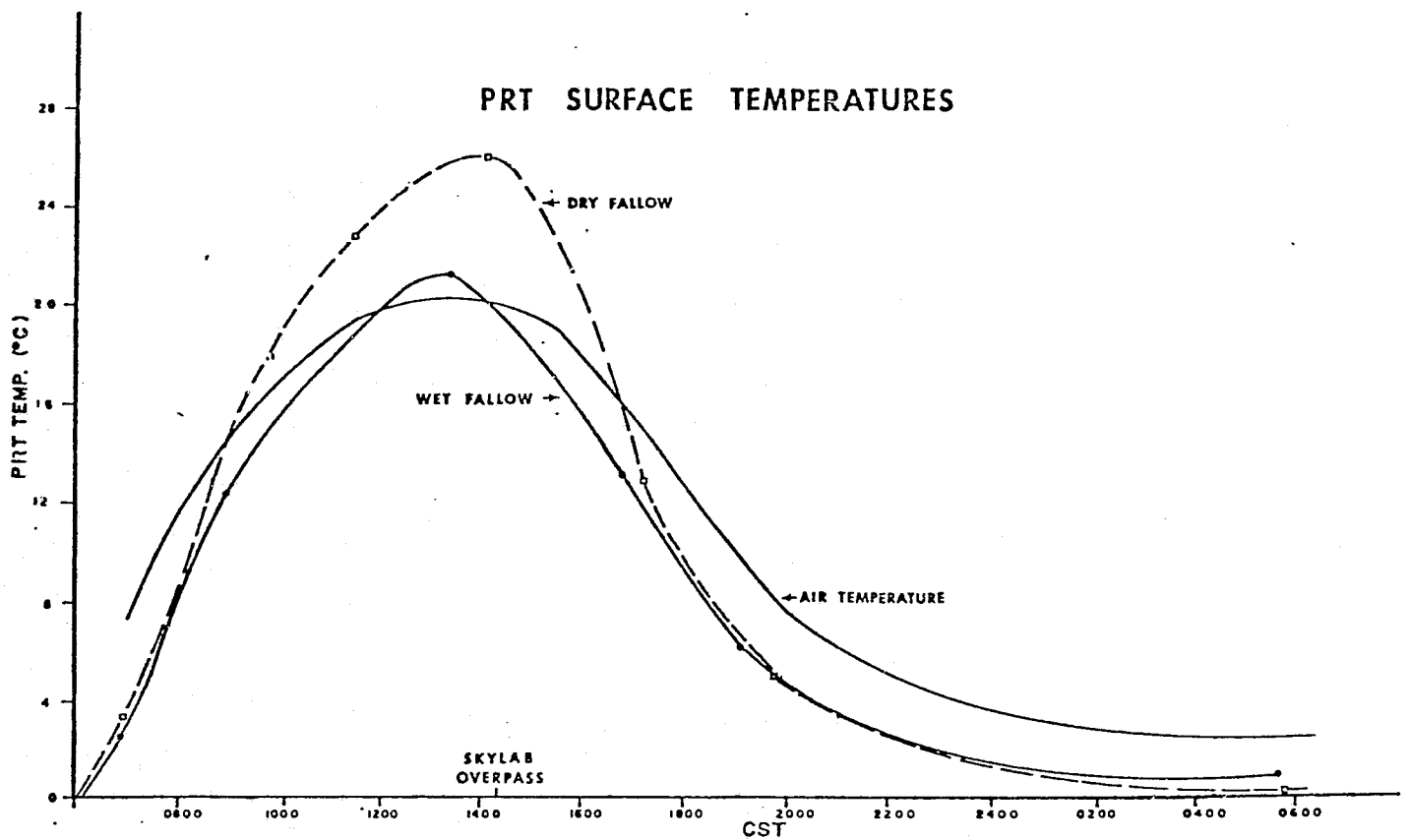

Fig. 15 - Diurnal equivalent blackbody surface temperatures as measured with a quantitative hand-held radiation thermometer for wet and dry fallow fields, #7 and #13, respectively.

the test site is presented in Fig. 16. The light (cool regions) in the RS-7 scanner data collected with the RB-57F aircraft include both irrigated lands and surface water. In this region, the area covered by surface water is small compared to the area of irrigated lands. Notice the remaining fields which are used for intensive agriculture that are not under irrigation on this date. The area covered by this single image is approximately 300 km^2 (117 $miles^2$). The same survey can be conducted with the SKYLAB data presented in Fig. 17. This single image represents a survey of approximately 1000 km^2 (390 $mile^2$).

Use of Remote-Sensor Data for Regional Water Budgets

Two approaches to monitoring regional soil moisture can be utilized with remote-sensor data. One approach is to assess the actual soil moisture level by observing crop and soil emittance and reflectance variations. The second is to assess evaporative losses as an input into the water budget.

The water budget approach [equation 13] requires an estimate of evapotranspiration and soil water flux. Present methods approximate the flux with known ground conditions and approximate the LT losses using a method such as the Jensen-Haise predictive model. The soil water flux term can be considerable for certain soils. Unless the flux term can be accurately predicted, effective use of water budgets is limited. The ET_p models have limitations for predicting actual ET of crops under stress due to water deficits but can be used for well-watered surfaces where the potential ET effectively predicts actual ET. Thus, remotely sensed data can, in conjunction with predictive ET models, be used to survey wet and dry regions which may include an irrigation district, a watershed, or other political or geographic areas. Approximations of actual evapotranspiration rates on a pixel, field, or regional basis may be used to further refine the technique.

The assumption that the air temperature in the Jensen-Haise model could be replaced with an apparent surface emittance, as measured by a remote sensor was required. A similar assumption could be incorporated for the measurement of R_s. The assumptions used to relate emittance to evaporative flux using the Jensen-Haise model may be replaced with ground control and with measurements of actual evaporative fluxes for

Fig. 16 - Survey of irrigated lands using the RB-57F, RS-7 scanner data. Area imaged is comparable to the photographic image in Fig. 1. The irrigated lands and surface water appear light in tone (cool). Approximate scale 1:100,000.

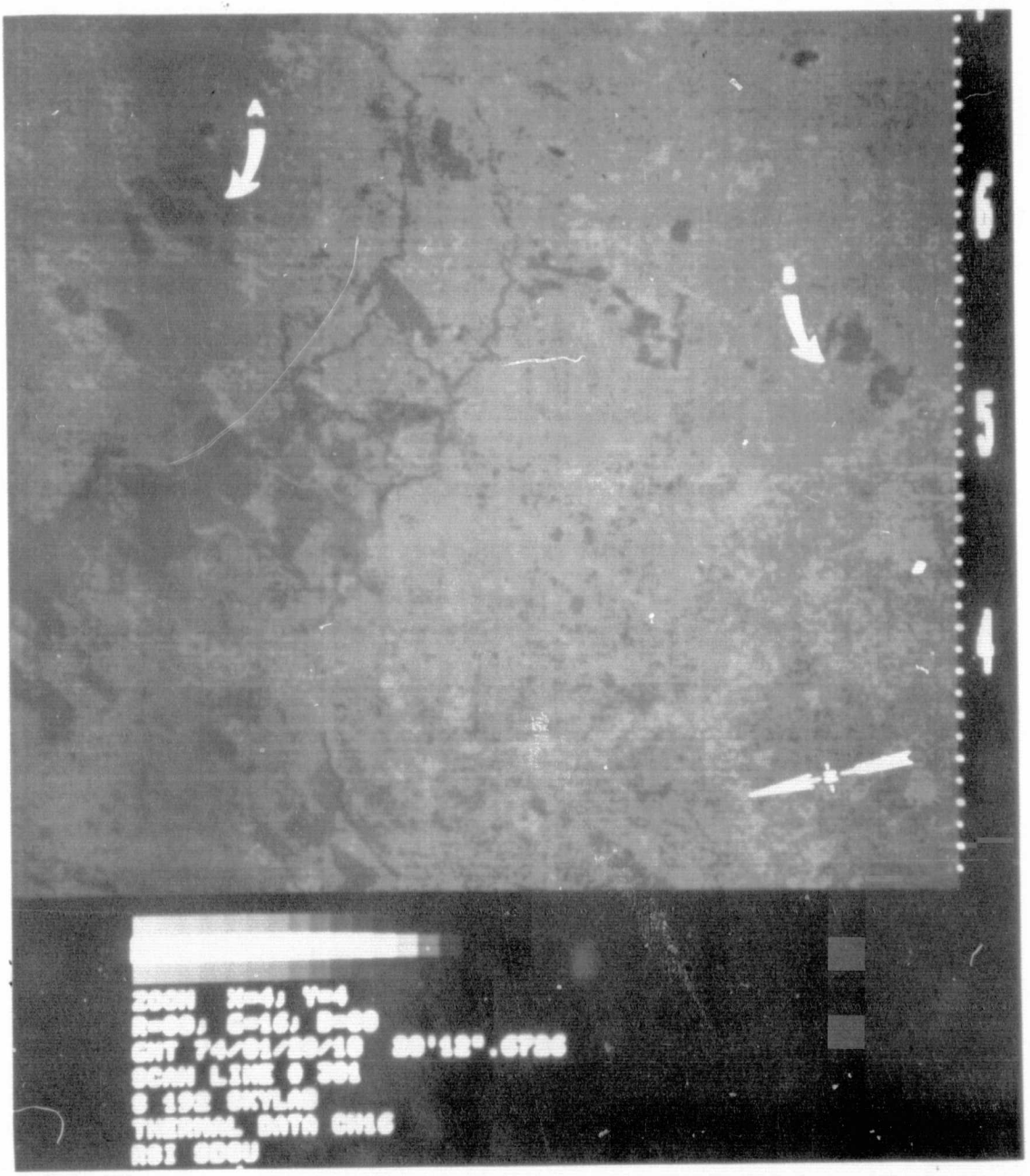

Fig. 17 - Survey of irrigated land using a DAS product of the thermal band from the S192 scanner on SKYLAB. The dark tones are either surface water or irrigated lands. Note the arrows identifying the location of the intensive test site. Approximate scale 1:200,000 (original in color).

equation calibration. The actual quantitative soil moisture prediction was suitable on fallow surfaces, but for vegetated surfaces for the data analyzed, the accuracy of prediction was not suitable for quantitative assessment. The use of remotely measured emittance and reflectance has promise for assessment of the similar type coefficient as crop coefficient which is presently used for relating the actual to predicted ET. The repetitive-coverage capabilities of satellite sensors observes not only the phenological advances of the crop canopies but also these phenological stages at various soil moisture levels. The concept certainly merits further investigation.

Remote-Sensor Data for Irrigation Scheduling

The use of potential evapotranspiration prediction models such as that by Wiegand and Bartholic (1970) can provide estimates of ET for well-watered surfaces. The remote assessments of R_n (net radiation) and T_o (surface temperature) are required. If remote sensing were used in an irrigation district where the crops were of the same species and the same phenological stage, the R_n, S (soil heat flux), and T_a (air temperature) would be of similar magnitudes. Therefore, the ET_p would be inversely proportional to a term which is a function of temperature. With ground control points of known ET, the temperature data alone could be calibrated to provide quantitative ET estimates. When the land use varies, assumption of equal values for R_n and S would not hold. However, as the soil water deficit increases to the level where the ET rate is decreased, the use of remotely monitored emittance variations for prediction of which fields are under stress may provide the input required for irrigation scheduling.

As soil water depletes, the assumptions required to apply the predictive ET_p equations do not hold so that the ET_p estimate becomes invalid as an estimate of actual ET. However, refering to the general energy budget equation [6], for a given amount of net radiation on surfaces where divergence terms can be neglected, the energy is utilized in soil heat flux (S), sensible heat flux to the air (A), and latent heat flux (E). As the latent heat flux decreases due to soil water deficits, the soil heat flux and sensible heat flux must increase to maintain the budget. These terms are both dependent upon temperature

gradients for heat transfer. Therefore, as E decreases with the same R_n, a larger temperature gradient from the surface must occur to appreciably increase A and S. This results in increased surface temperatures which can be monitored as emittance variations with remote sensors. Carson (1961) illustrated that as the 0→45 cm soil moisture decreased from 4 cm to 1.9 cm of stored moisture the proportion of R_n used as E (or $\frac{E}{A+S+E}$) decreased from 81%→14%. Therefore, greater surface temperatures were associated with the dryer conditions for the transport of the heat by A and S. The unique feature of heat dissipation by latent heat is that the heat is utilized in the heat of vaporization with the transfer from the surface as a transfer of vapor. The vapor transport is dependent upon vapor pressure deficits in contrast to temperature gradients. Therefore, the predictive ET_p models do not require a quantitative prediction of the actual ET rate but can be used with ground control in irrigation scheduling with surface emittance assessments for determing when soil-water deficits are limiting to the crop.

An example evaluation of utilizing the remote surface emittance measurements for irrigation scheduling within a crop species can be illustrated using alfalfa fields #3, 4, 5, 11, and 12. Even when significant correlations of S192 and soil moisture were not obtained for all cropped fields, the alfalfa fields were statistically classed into three separate categories -- #3, 12 versus #5 versus #4, 11. These corresponded with composite moisture values of 15.1%, 18.0%, and 24.1%, respectively. Therefore, the emittance variations could be used to classify the alfalfa fields into moisture categories.

Requirements for Data Handling in Operational Irrigation Scheduling Procedures

Most applications of remote sensing require the relative comparisons of ground features for the specific evaluation. For irrigation scheduling or soil moisture assessments, the state-of-the-art technology is to compare the known with an unknown by using the known to calibrate predictive equations (the example multiple regressions in Table 16). Therefore, methods of accurately locating and registering ground to aerial data and of reducing the aerial data to represent the ground scenes

are required. In irrigated regions, the soil moisture variations are associated with irrigation scheduling which is based upon field variations. Therefore, the method for data reduction developed in this activity is well suited to operational programs. The method includes location of field boundaries, computing statistics of the fields, and using a statistical classification which uses means and variances with probability theory for establishing significant differences. The use of gradient thresholds to remove high gradient or transitional radiometric information from the statistics is especially an advantage for comparatively low-resolution satellite data. Data should be included from as much of the field as possible to yield an optimal representation of the field in question. The pixels at field margins represent data mixtures in contrast to observations of only one data class. When these points are deleted from the set of data used to compute the means and variances, the mean is representative of the field without being partially dependent on the adjacent areas.

An example use of the procedures in irrigation scheduling of similar species of crops would include the monitoring of ground control fields which are in various irrigation or soil moisture stages. The digital data can be quickly reduced to locate fields which are radiometrically different than their surroundings, compute the statistics, and statistically compare the fields with the ground control fields to determine, at the confidence level selected by the resource manager, the statistical differences of the field means, thereby, classifying the fields as to their irrigation requirements.

CONCLUSIONS

1. Wavelengths greater than 2.1 μm were required to spectrally distinguish between wet and dry fallow surfaces.

2. Thermal data provided a better estimate of soil moisture than did data from the reflective bands.

3. Thermal data were dependent on soil moisture but not on the type of agricultural land use.

4. The emittance map, when used in conjunction with existing models, did provide an estimate of evapotranspiration rates. A method to use remote thermal data to replace the crop coefficients for relating actual ET to predicted ET should be evaluated.

5. Surveys of areas of high soil moisture can be accomplished with space altitude thermal data. If both soil moisture and land use are to be surveyed, at least one reflective channel must be included in the analysis.

6. Thermal data will provide a reliable input into irrigation scheduling.

7. The thermal and spatial resolution of the S-192 X/5 detector SKYLAB data is appropriate for monitoring soil moisture and for irrigation scheduling.

8. Time of data collection for soil moisture surveys should be close to midday.

9. At least the 10.2→12.5 μm, 1.55→1.75 μm, 0.98→1.08 μm, and 0.56→0.61 μm spectral regions should be included on operational space-altitude scanners for soil moisture applications.

10. Predictive regression equations using S192 data as independent variables had multiple correlation coefficients as large as 0.947 and 0.737 for predicting soil moisture of fallow and cropped surfaces, respectively.

LIST OF REFERENCES

Bartholic, J.R., L.N. Namken, and C.L. Wiegand. 1970. Combination equations used to calculate evaporation and potential evaporation. ARS 41-170 USDA. 14 pp.

Black, T.A., W.R. Gardner, and C.B. Tanner. 1970. Water storage and drainage under a row crop on a sandy soil. Agronomy Journal 62:48-51.

Bowen, I.S. 1926. The ratio of heat losses by conduction and by evaporation from any water surface. Physical Review 27:780-787.

Carson, J.E. 1961. Soil temperature and weather conditions. Argonne National Laboratory. Report ANL-6470. Argonne, Illinois. 244 pp.

DeVries, D.A. 1963. Thermal Properties of Soils. In Physics of Plant Environment. ed W.R. Van Wyk. North-Holland Publishing Company. Amsterdam.

Goltz, S.M., C.B. Tanner, A.A. Millar, and A.R.G. Lang. 1971. Water balance of a seed onion field. Agronomy Journal 63:762-765.

Idso, S.B., R.D. Jackson, and R.J. Reginato. 1975. Detection of soil moisture by remote surveillance. American Scientist 63(5):549-557.

Jensen, M.E. and H.R. Haise. 1963. Estimating evapotranspiration from solar radiation. American Society of Civil Engineering Proceedings, Journal of Irrigation and Drainage Division. 89:15-41.

Juday, R.D. 1974. Intricate Alignment and Timing Facts for S191. JSC, Houston, Texas.

Lockwood, N.E. 1974. SL/4 Sensitometric Data Package. NASA Report #JL 12-505. Houston, Texas.

McGuinnes, J.L., and E.F. Bordne. 1972. A comparison of lysimeter-derived potential evapotranspiration with computed values. ARS-USDA Technical Bulletin No. 1452, U.S. Government Printing Office. 71 pp.

Moore, D.G., M.L. Horton, and M.J. Russell. 1974. Preliminary evaluation of S-192 SKYLAB data for assessing energy exchange and land use in irrigated agriculture. Interim report to NASA Contract NAS 9-13337. Remote Sensing Institute Report Number RSI-SDSU-74-18, South Dakota State University, Brookings, South Dakota. 58 pp.

Morton, F.I. 1969. Potential evaporation as a manifestation of regional evaporation. Water Resources Research 5(6):1244-1255.

Rosenberg, N.J., H.E. Hart, and K.W. Brown. 1968. Evapotranspiration: review of research. University of Nebraska MP20, Lincoln, Nebraska. 80 pp.

Sellers, W.D. 1965. Physical climatology. The University of Chicago Press. Chicago.

Soil Conservation Service. 1972. General soil map of Dimmit and Zavala Counties, Texas. U.S. Department of Agriculture. Temple, Texas.

Stone, L.R. and M.L. Horton. 1974. Estimating evapotranspiration using canopy temperatures; field evaluation. Agronomy Journal 66:450-454.

Tanner, C.B. 1960. Energy balance approach to evapotranspiration from crops. Soil Science Society of American Proceedings 24:1-8.

Tanner, C.B. 1963. Plant temperatures. Agronomy Journal 55:210-211.

Werner, H.D. and F.A. Schmer. 1972. Application of remote sensing techniques to cropland and rangeland soil water inventory. Remote Sensing Institute Report RSI-72-16. Final Report to U.S. Geological Survey.

Wiegand, C.L. and J.F. Bartholic. 1970. Remote sensing in evapotranspiration research on the great plains. In Evapotranspiration on the Great Plains. Publication Number 50, Kansas State University. pp. 137-180.

Wiegand, C.L. and L.N. Namken. 1966. Influences of plant moisture stress, solar radiation, and air temperature on cotton leaf temperature. Agronomy Journal 58:582-586.

APPENDIX A

TABLE A-1. SENSOR DESCRIPTION AND PLACEMENT FOR GROUND DATA COLLECTION.

Sensor	Measurement	Depth (in cm)[1/]
Eppley precision pyranometer	0.258→2.8 μm	incoming
Precision radiation thermometer	8→14 μm	surface
Net radiometer	total net	surface
Mark IG radiometer	0.35→1.15 μm	surface
	0.52→1.15 μm	surface
Mark IRF radiometers	0.60→1.15 μm	surface
	0.71→1.15 μm	surface
Soil heat flux plates	soil heat flux	-5
Soil temperature	thermocouple	0, -2.5, -5, -7.5, -20, -40, -60, -100
Air temperature	shielded thermocouple	+20, +40, +80, +160, +240, +320
Humidity	atkins	+100

[1/] where "-" is below the land surface and "+" is above the land surface.

TABLE A-2. AERIAL DATA COLLECTION.

Location	Platform	Date	Film/Filter									Thermal Scanner	Multi spectral Scanner	RAD/SCAT
			RC8		Zeiss	Hasselblad								
			6"	6"	12"	1	2	3	4	5	6			
Carrizo Springs, Texas	NC-130B	1/28/74	So-397 HF3	2443 15		2402 58	2402 25	2424 89B	So-356 HF3	2443 12			✓	✓
Carrizo Springs, Texas	RB-57F	1/28/74	So-397 2A	2443 510NM	2443 12	2402 57	2402 25	2424 89B	2424 87	2443 12		✓		
Timber Lake, South Dakota	HC-130B	6/13/73	So-397 2E	2443 510NM		2402 58	2402 25	2424 89B		2443 12	So-356 HF3	✓	✓	
Timber Lake, South Dakota	RSI-Beachcraft Night Mission	6/9/73										✓		
Timber Lake, South Dakota	RSI-Beachcraft	6/10/73				2402 58	2402 25	2424 89B		2443 15		✓		
Pierre, South Dakota	NC-130B	9/18/73	So-397 2A	2443 12						2443 12	So-356	✓	✓	
Pierre, South Dakota	RSI Beachcraft Night Mission	9/18/73										✓		
Pierre, South Dakota	RSI-Beachcraft	9/18/73				2402 58	2402 25	2424 89B		2443 15		✓		

TABLE A-3. RADIOMETRIC VALUES FOR EACH OF THE 31 TEST SITES FROM THE S190-A CAMERA SYSTEM. FIELD NUMBERS CORRESPOND TO THOSE IN FIG. 2 AND TABLE 1.

Field No.	Radiance Values for Each Spectral Region*			
	0.5-0.6μm	0.6-0.7μm	0.7-0.8μm	0.8-0.9μm
1	0.125	0.134	8.692	6.462
2	0.144	0.155	7.934	6.462
3	0.161	0.172	8.692	6.389
4	0.176	0.213	6.022	4.472
5	0.183	0.222	6.551	4.648
6	0.150	0.155	11.890	7.528
7	0.140	0.151	11.730	7.063
8	0.115	0.124	9.098	6.302
9	0.208	0.216	24.820	11.150
10	0.142	0.151	10.870	6.967
11	0.179	0.222	6.641	4.886
12	0.130	0.146	10.730	6.967
13	0.135	0.146	10.730	6.626
14	0.144	0.142	11.540	8.975
15	0.142	0.137	11.890	6.160
16	0.130	0.139	11.380	7.916
17	0.146	0.144	16.350	5.860
18	0.162	0.176	8.975	5.940
19	0.152	0.162	7.511	6.794
20	0.162	0.162	10.410	6.967
21	0.150	0.144	9.245	4.712
22	0.134	0.142	7.308	6.231
23	0.125	0.103	6.317	6.967
24	0.162	0.164	7.614	6.717
25	0.159	0.151	6.091	7.143
26	0.152	0.153	12.080	7.426
27	0.148	0.151	11.050	8.006
28	0.152	0.141	7.614	7.426
29	0.146	0.153	9.655	7.143
30	0.155	0.162	9.811	5.940
31	0.162	0.149	12.450	6.794

* All values reported have exponent of 10^{-3} for cal cm^{-2} min^{-1}.

TABLE A-4. RADIOMETRIC MEAN VALUES FOR EACH OF THE 31 TEST SITES FROM THE S192 SCANNER. FIELD NUMBERS CORRESPOND TO THOSE IN FIGURE 2 AND TABLE 1.

Field No.	Radiance Values for Each Spectral Region*								
	0.56→0.61μm Channel 3-4	0.68→0.76μm Channel 7-8	0.78→0.88μm Channel 9-10	0.98→1.08μm Channel 19	1.09→1.19μm Channel 20	1.55→1.75μm Channel 12	2.1→2.35μm Channel 13-14	10.2→12.5μm Channel 15-16	10.2→12.5μm Channel 21
1	5.181	5.104	1.670	3.568	2.054	8.295	0.404	0.857	0.856
2	4.078	3.690	3.747	3.217	1.347	5.063	0.150	0.801	0.803
3	3.588	5.004	4.277	3.433	2.214	7.803	0.285	0.865	0.855
4	2.587	5.877	3.477	5.841	2.762	5.053	0.084	0.819	0.818
5	3.667	3.820	3.229	2.958	1.761	6.634	0.261	0.846	0.838
6	3.413	3.303	3.928	2.539	1.156	6.950	0.326	0.840	0.837
7	4.798	4.345	3.796	3.208	1.669	6.143	0.180	0.796	0.800
8	4.520	5.625	4.133	4.124	2.388	8.163	0.352	0.867	0.849
9	0.249	0.085	3.188	0.053	0.043	0.032	0.009	0.749	0.757
10	3.790	2.832	3.580	2.366	1.281	5.304	0.159	0.795	0.810
11	3.601	4.146	3.641	3.008	1.286	6.043	0.224	0.808	0.812
12	5.250	3.844	3.191	2.518	1.777	8.615	0.470	0.886	0.874
13	5.500	3.428	2.691	1.993	1.308	9.048	0.555	0.892	0.882
14	3.187	4.974	8.159	3.596	1.590	0.769	0.156	0.834	0.822
15	3.654	4.094	3.398	3.277	1.819	1.473	0.327	0.859	0.855
16	5.135	5.918	5.489	3.690	2.494	1.725	0.465	0.887	0.910
17	4.061	6.349	8.994	4.523	1.922	1.671	0.268	0.812	0.855
18	2.352	2.244	2.684	8.014	2.047	0.277	0.163	0.844	0.793
19	4.323	5.387	5.419	3.601	2.412	1.655	0.359	0.849	0.787
20	5.165	5.166	5.097	3.447	2.274	1.264	0.443	0.858	0.842
21	2.244	4.999	9.295	2.324	1.466	0.933	0.017	0.802	0.846
22	3.533	4.482	4.170	4.252	2.274	1.647	0.269	0.835	0.867
23	2.848	5.770	7.179	2.975	1.644	0.989	0.116	0.811	0.812
24	4.517	2.216	0.305	1.310	6.775	1.783	0.385	0.854	0.858
25	4.354	7.054	10.132	1.355	1.939	1.652	0.271	0.824	0.879
26	4.483	5.488	5.266	4.514	2.296	1.612	0.431	0.855	0.822
27	5.059	4.289	3.919	4.062	1.336	1.345	0.404	0.873	0.826
28	5.720	5.362	4.777	0.987	0.695	1.106	0.523	0.892	0.867
29	5.235	6.288	6.322	4.396	2.047	1.814	0.440	0.878	0.841
30	5.624	6.478	6.567	2.708	1.750	1.613	0.458	0.872	0.886
31	4.380	5.151	5.103	2.804	1.577	1.280	0.389	0.889	0.863

*All values reported have exponent of 10^{-3} for cal cm^{-2} min^{-1}.

TABLE A-5. RESULTS OF THE t-TEST USING MEAN RADIANCE VALUES FOR FIELDS FROM THE SCANNER OF THE NC-130B AIRCRAFT. CLASSES ARE STATISTICALLY DIFFERENT FOR EACH SPECTRAL BAND USING A 0.05 CONFIDENCE LEVEL.

Class Number	0.38-0.45µm Ch-1 Field(s)	0.41-0.45µm Ch-2 Field(s)	0.45-0.52µm Ch-3 Field(s)	0.54-0.58µm Ch-4 Field(s)	0.59-0.64µm Ch-5 Field(s)	0.65-0.69µm Ch-6 Field(s)	0.71-0.76µm Ch-7 Field(s)	0.77-0.81µm Ch-8 Field(s)	0.83-0.88µm Ch-9 Field(s)	0.38-1.34µm Ch-10 Field(s)	1.20-1.30µm Ch-11 Field(s)	1.53-1.63µm Ch-12 Field(s)	2.10-2.38µm Ch-13 Field(s)	8.5-8.9µm Ch-17 Field(s)	9.5-10.2µm Ch-19 Field(s)	10.2-11.0µm Ch-20 Field(s)	11.2-11.9µm Ch-21 Field(s)	12.2-13.0µm Ch-22 Field(s)	1.14-1.16µm Ch-23 Field(s)	1.05-1.09µm Ch-24 Field(s)
1	8	7, 8	8, 7	7	7, 8	7, 8	4,11	4,11	11, 4	11, 4	4	1	8	12	12	13	13,12	13,12	4,11	5, 4
2	1	1,13	1,13	8	1,13	1,13	5	5	5	5	3	8	13; 1	3	3,13	12	3, 8	8	5.1.7.8	11, 5
3	10	6	6	1,13	6, 2, 10	6, 2, 12	7, 2, 3	3	3, 7, 1	7, 3	11, 5, 7	13	6,12	13	1, 8	3, 8	1	1, 3	13, 3	7
4	13, 6	10,12	10,12	6, 2	12	10	2, 1	7, 2, 1, 8, 13,12, 6,10	2, 8	8	13, 1	12	3	1	6, 5	1	6	6	12,10, 2	8
5	2, 7	2	2	10,12	3	3	13,12	-	13,12	1, 2, 13	3	6, 3	7, 2	8	4, 2	6	5	5	6	3,12
6	12	3	3	3	4	4, 5	10, 6	-	10	12	12, 2	2, 4, 7,10,5	10	6, 5	7,10, 11	5	4	4	-	13, 2, 10, 1
7	3, 4	4	4	4	5	11	-	-	6	10, 6	10, 6	11	4, 5	4	-	4	2,11	11, 2	-	-
8	11, 5	6, 5	5	5	11	-	-	-	-	-	-	-	11	11	-	11,-2	10	7,10	-	-
9	-	11	11	11	-	-	-	-	-	-	-	-	-	2	-	10	7	-	-	-
10	-	-	-	-	-	-	-	-	-	-	-	-	-	7	-	7	-	-	-	-
11	-	-	-	-	-	-	-	-	-	-	-	-	-	10	-	-	-	-	-	-

APPENDIX B

EDGE DETECTION COMPUTER PROGRAM

The subroutines required to implement the edge detection program are MASMOV, HISPLT, and SYMFRQ, which may be obtained upon request.

```
C         PARAMATER CARD
      DIMENSION IRB(2)
      INTEGER*4 LINEPK(512),IOFREQ(256),IGFREQ(256)
      INTEGER*4  ALABEL(20),MEDG4(512)
      INTEGER*2 M2
      LOGICAL*1 LINE,LIN3(2)
      LOGICAL*1  LIN1(2048),LIN2(2048),MEDG1(2048)
      EQUIVALENCE (MEDGE(1),MEDG1(1),MEDG4(1))
      INTEGER*2  MLIN1(1024),MLIN2(1024),MLIN3(1)
      EQUIVALENCE (MLIN3(1),LIN3(1))
      DIMENSION   NUM1(16),NUM2(16),NUM3(16)
      INTEGER*2    IDIR(1024,10),MRBGR2(1024,10),MEDGE(1024)
      INTEGER*2  NSUM2(1024)
      INTEGER*2  NSUM1(1024)
      COMMON /KLENG/ILEN/KCALL/ICALL
      COMMON /INPUT/LINE(2048)
      EQUIVALENCE    (MLIN1(1),LIN1(1))
      EQUIVALENCE    (MLIN2(1),LIN2(1))
      EQUIVALENCE (LINE(1),LINEPK(1))
      DATA  NUM1/1,2,3,4,5,1,2,3,4,5,1,2,3,4,5,1/
      DATA  NUM2/2,3,4,5,1,2,3,4,5,1,2,3,4,5,1,2/
      DATA  NUM3/3,4,5,1,2,3,4,5,1,2,3,4,5,1,2,3/
      DATA  IOFREQ/256*0/,IGFREQ/256*0/
      ICR=11
      LP=12
      MAGIN=14
      MAGOU=15
C.........MXI.....STARTING HORIZONTAL BYTE NUMBER.
C.........MXF.....STOPPING HORIZONTAL BYTE NUMBER.
C.........MYI.....STARTING VERTICAL LINE NUMBER.
C.........MYF.....STOPPING VERTICAL LINE NUMBER.
C.........NFRQ....CONTROL FOR HISTOGRAM OUTPUT.
C.........          1...AND...2     NO INDIVIDUAL COUNT ONLY BAR GRAPH.
C.........          3...ONLY INDIVIDUAL AND CUMLITIVE COUNT NO BAR GRAPH.
C.........          4...AND ABOVE   BOTH BAR GRAPH AND COUNT.
C.........LRBGR...GRADIANT THREHOLD THAT WANT TO KEEP PERMANNATLY ON
C.........          FILE, ANYTHING LOWER THAN THIS IS SET TO ZERO(0).
C.........NPRT....IF GRADIANT OUTPUT IS NOT WANTED SET EQUAL TO ONE,
C.........          OTHERWISE ANY NUMBER INCLUDING ZERO.
      READ(ICR,1000)MXI,MXF,MYI,MYF,NFRQ,LRBGR,NPRT,NDIRGR
      MXF4=MXF/4
      MXF=MXF4*4
      NR=MYF-MYI
      GO TO(108),MYI
      MYI=MYI-1
      DO 100 II=1,MYI
  100 READ(MAGIN,1001)
  108 ILEN=MXF-MXI+1
      KM=ILEN-1
```

```
      KML=ILEN-2
      NNN=31
      ICALL=1
      IYY=MYI+2
      MX=MXI+1
      NST=MXI-1
      ILEN2=ILEN*2
      K4=KM/4
      III=0
      DO 104 I=1,NR
      III=III+1
      READ(MAGIN,1001)(LINEPK(J),J=1,MXF4)
      CALL MASMOV(ILEN,LINE(MXI),LINE(1))
      LIN3(2)=LINE(1)
C.....SUMS TWO PIXELS TOGETHER ACROSS THE LINE.
      DO 51 IT2=4,ILEN2,2
      IT=IT2-2
      ITT=IT/2
      IT8=ITT+1
      M2=MLIN3(1)
      LIN3(2)=LINE(IT8)
   51 NSUM2(ITT)=M2+MLIN3(1)
      GO TO(14,15,16,10,10,10,12,12,12,12,12,12,13),III
   13 III=8
C        SECTION FOR LOCATING EDGES
   12 IBND=III-1
      I1=NUM1(IBND)
      I2=NUM2(IBND)
      I3=NUM3(IBND)
      IYY=IYY+1
C.....CHECK EACH POINT FOR LOCAL MAXIMUM ACROSS THE LINE.
      DO 22 IT=2,KML
      ICX=0
      ITPLUS= IT+1
      ITMIN=IT-1
      IDX=IDIR(IT,I2)
      IRBM=MRBGR2(IT,I2)
      IF(IRBM.LT.LRBGR)GO TO 25
      GO TO (24,28,26,23,24,28,26,23),IDX
C.....CHECK FOR LOCAL MAXIMUM IN DIAGONNAL DIRECTION.   UR TO LL
   23 IRB1=IRBM-MRBGR2(ITPLUS,I1)
      IRB2=IRBM-MRBGR2(ITMIN,I3)
      IF(IRB1)22,41,41
   41 IF(IRB2)22,61,61
   61 CONTINUE
      GO TO 21
C.....CHECK FOR LOCAL MAXIMUM .   ABOVE AND BELOW
   24 IRB1=IRBM-MRBGR2(IT,I1)
      IRB2=IRBM-MRBGR2(IT,I3)
      IF(IRB1)22,43,43
   43 IF(IRB2)22,62,62
   62 CONTINUE
      GO TO 21
C.....CHECK FOR LOCAL MAXIMUM DIAGONNAL DIRECTION .   UL TO LR
```

```
   28 IRB1=IRBM-MRBGR2(ITMIN,I1)
      IRB2=IRBM-MRBGR2(ITPLUS,I3)
      IF(IRB1)22,45,45
   45 IF(IRB2)22,63,63
   63 CONTINUE
      GO TO 21
C.....CHECK FOR LOCAL MAXIMUM.    RIGHT AND LEFT
   26 IRB1=IRBM-MRBGR2(ITPLUS,I2)
      IRB2=IRBM-MRBGR2(ITMIN,I2)
      IF(IRB1)22,47,47
   47 IF(IRB2)22,64,64
   64 CONTINUE
   21 ICX=IRBM
C.....MAXIMUM GRADIANT VALUE IS 255.
      IF(ICX.GT.255)ICX=255
   25 CONTINUE
    2 CONTINUE
   22 MEDGE(ITMIN)=ICX
      DO 73 IP=2,ILEN2,2
   73 MEDG1(IP/2)=MEDG1(IP)
      MX=1
      NNN=31
      GO TO(986),NPRT
C.....WRITE OUT GRADIANT TO TAPE.
      WRITE(MAGOU,1001)(MEDG4(IT),IT=1,K4)
  986 CONTINUE
      CALL SYMERO(0,ITMIN,MEDGE(1),IGFREQ)
C        GRADIENT SECTION
C.....DETERMINE DIRECTION AND GRADIANT FOR EACH POINT.
   10 I1=NUM1(III-3)
      DO 52 IT=1,KM
      IT2=IT+1
      X=MLIN1(IT2)-MLIN2(IT)
      Y=MLIN1(IT)-MLIN2(IT2)
      IDIR(IT,I1)=IDIRX(X,Y)
      GGRAD=  ABS(X)+ABS(Y)
   52 MRBGR2(IT,I1)=GGRAD
C.....MOVES AVERAGES FORM ARRAY TWO TO ARRAY ONE.
   16 CALL MASMOV(ILEN2,LIN2(1),LIN1(1))
C.....ADD SUM OF TWO ROWS TOGETHER DIVIDE BY FOUR. AVERAGES FOR A
C.....          FOUR PIXEL ARRAY.
   15 DO 74 IT=1,ILEN
   74 MLIN2(IT)=(NSUM2(IT)+NSUM1(IT))/4
C.....MOVES SUM FROM ARRAY TWO TO ARRAY ONE.
   14 CALL MASMOV(ILEN2,NSUM2(1),NSUM1(1))
  104 CONTINUE
      WRITE(LP,1009)ITMIN,IYY
      IGFREQ(1)=0
      READ(ICR,1003,END=110) ALABEL
C.....PLOTS HISTOGRAM OF OUTPUT.
  110 CALL HISPLT(IGFREQ,ALABEL,NFRQ)
 1000 FORMAT(815)
 1001 FORMAT(200(12A4))
 1002 FORMAT(' ',32I4)
```

```
1003 FORMAT(20A4)
1004 FORMAT('1',10X,20A4)
1005 FORMAT(' ',5X,'ELEMENT ',I5,'LINE ',I5,73X,'ELEMENT ',I5,'LINE ',I
    15)
1006 FORMAT(200(50A1))
1009 FORMAT(' ',10X,'THERE ARE',I4,' ELEMENTS USED,AND ',I4,' LINES')
     END
     FUNCTION IDIRX(X,Y)
     IF(.NOT.(X.EQ.0.AND.Y.EQ.0))GO TO 5
     IDIRX=0
     RETURN
   5 IF(X.EQ.0)X=.001
     RAT=Y/X
     IF(.NOT.(RAT.GT..4142.AND.RAT.LT.2.4142))GO TO 1
     IDIRX=2
     IF(Y.LT.0)IDIRX=6
     RETURN
   1 IF(.NOT.(RAT.LT.-.4142.AND.RAT.GT.-2.4142))GO TO 2
     IDIRX=4
     IF(X.GT.0)IDIRX=8
     RETURN
   2 RAT=ABS(RAT)
     IF(RAT.LT.2.4142)GO TO 3
     IDIRX=3
     IF(Y.LT.0)IDIRX=7
     RETURN
   3 IDIRX=1
     IF(X.LT.0)IDIRX=5
     RETURN
     END
```

ADJACENCY METHOD COMPUTER PROGRAM

The subroutines required to implement the adjacency classifier program are REDAPE, MASMOV, CLSAPE, which may be obtained upon request.

```
C*****************************************************************
C        PROGRAM NAME.....ADJACENCY CLASSIFIER
C        OCTOBER 2,1975
C        WRITTEN BY  MIKE RUSSELL
C*****************************************************************
C        CONTROL SECTION
      DIMENSION     MADJ(512)
      DIMENSION    LINSUM(1024,3)
      INTEGER*4 LS(256)
      INTEGER*4 NUM,SUM,SUM2
      INTEGER*2LINE,LIN1(1024),LA,DEC,DEC1(1024),LINDUP(1024)
      LOGICAL*1  LC,A(512)
      COMMON NUM(256,2),SUM(256,2),SUM2(256,2),IBG,ICD,II,LA(2048)
      COMMON DEC(1024),LC(256)
      COMMON /INPUT/LINE(1024)
      EQUIVALENCE (DEC1(1),LC(1))
      EQUIVALENCE (LA(1),A(1))
      EQUIVALENCE (LINDUP(1),LINE(1))
C        INITIALIZE CONSTANTS AND SET LIMITS
C*****************************************************************
C        OFFSET INTO TRANSLATION TABLE
      ITAB=0
C
C        ICD IS THE STARTING CLASS
C        CLASSES 1-4 ARE RESERVED FOR EDGES
C        CLASS  5  IS RESERVED FOR INSIGNIFICANT CLASSES
      ICD=5
      IBG=ICD
C        ID & IDD ARE VARIABLES TO CONTROL SEARCHING TECHNIQUE(IFLG)
      ID=1
      IDD=2
C        ICR=NUMBER OF CARD READER
C        LP= NUMBER OF WRITER
C        MDIN=NUMBER OF TEMPORARY FIELD NUMBER STORAGE AREA
C        MDOUT=NUMBER OF PERMANENT FIELD NUMBER  STORAGE AREA.
      ICR=5
      LP=6
      MDIN=8
      MDOUT=10
C        IERR=1  IMPLIES TRANSLATION TABLE IS FULL AFTER TRANSLATION
      IERR=2
C        INITIALIZE TRANSLATION
      LA(1)=1
      LA(2)=2
      LA(3)=3
      LA(4)=4
      LA(5)=5
 1004 FORMAT('0',' LINE='/32I4)
 1005 FORMAT('0',' IFLG=  ',I10,'  NUTS=',I10)
C        READ INITIAL DATA BLOCK LIMITS  (6I5)
      READ(ICR,1000)MXI,MXF,MYI,MYF,LRBGR,IAVE
C        MXI,MXF  IS THE LOCATION OF THE INITIAL POINT
C        MYI,MYF IS THE LOCATION OF THE FINAL POINT
C        LRBGR IS THE GRADIENT THRESHOLD
C        NREC IS THE NUMBER OF ROWS MINUS  ONE   FROM THE DATA
C        IAVE   IS THE NUMBER OF DATA LINES AVERAGED
      NREC=MYF-MYI
C        ZERO THE   NUM,SUM,& SUM2
      DO 200 I=1,256
      NUM(I,1)=0
      SUM(I,1)=0
  200 SUM2(I,1)=0
C
C        START THE LOOP OF READING DATA
C*****************************************************************
C        SKIP MYI DATA RECORDS AND READ ONE RECORD INTO COMMON/INPUT/
      DO 100 II=1,MYI
  100 CALL REDAPE(MXI,MXF,KM)
      K=KM
      MZ=2*K
      IIELEM=IAVE*IAVE
      II=0
```

```
C...  ...AVERAGE IAVE BY IAVE NEIGHBORHOODS FOR FIRST LINE.............
      GO TO(52),IAVE
      IIAV=IAVE-1
      K=KM-IAVE
      NZ=2*K
      DO 51 I=1,IAVE
      DO 50 J=1,K
      JMAX=J+IIAV
      DO 50 KK=J,JMAX
   50 LINSUM(J,I)=LINSUM(J,I)+LINE(KK)
   51 CALL REDAPE(MXI,MXF,KM)
      DO 55 J=1,K
      SUS=0.
      DO 54 I=1,IAVE
   54 SUS=SUS+LINSUM(J,I)
      LIN1(J)=SUS/IIELEM
   55 CONTINUE
      GO TO 53
   52 CALL MASMOV(NZ,LINDUP,LIN1)
   53 KD=K-1
      KP=K-1
      NZ=2*KD
      II=0
C...  ...WHEN DONE WITH DATA.....................................................
      DO 101 III=IAVE,NREC,IAVE
      DO 101 KKK=1,IAVE
      II=II+1
      CALL REDAPE(MXI,MXF,KM)
C...  ...AVERAGE NEXT LINE.....................................................
C...  ...OR  BRANCH AROUND LINE AVERAGE SECTION
      GO TO(773),IAVE
      DO 57 JJ=1,K
      LINSUM(JJ,KKB)=0
      JMAX=JJ+IIAV
      DO 58 KK=JJ,JMAX
   58 LINSUM(JJ,KKB)=LINSUM(JJ,KKB)+LINE(KK)
      SUS=0
      DO 59 KB=1,IAVE
   59 SUS=SUS+LINSUM(JJ,KB)
   57 LINE(JJ)=SUS/IIELEM
  773 IFLG=ID
      NADJ=4
      IFL= 1
      IGRNUM=2
C...  ...PROCESS A LINE OF DATA FOR ADJACENT CLASSES.....................
      DO 102 J=1,KO
      J2=J+1
      N=LIN1(J)
      Y=N-LINE(J2)
      X=LIN1(J2)-LINE(J)
C...  ...APPROXIAMATE MAGNITUDE OF GRADIENT VECTOR.....................
      Z=(X*X+Y*Y)**.5
      IRBGR=Z
C...  ...COMPARE GRADIENT MAGNITUDE TO THRESHOLD.....................
      IF(IRBGR-LRBGR)110,111,111
C...  ...IF GRADIENT IS LESS THAN THRESHOLD.....................
  110 GO TO(113,114,115,115),IFLG
C...  ...SEARCH POSITIONG A AND C FOR.....................FIELDS   C...
C...  ...FIELD NUMBERS ADJACENT TO B.....................      A B...
C        SECTION IFLG=3 OR 4
  115 IB=DEC(J)
C...  ...CHECK POSITION C  FOR INSIGNIFICANT FIELD NUMBERS.....................
      GO TO(509,509,509,509,516),IB
C        YES  THERE IS AN ADJ CLASS  (CHECK IF SAME AS BEFORE)
      GO TO(506),IFL
C        CONTINUE  (NO NEW ADJ)
      GO TO 114
  516 GO TO(519,519,519,519,519),NADJ
      GO TO 114
  519 NADJ=5
      GO TO 114
C       A NEW ADJ CLASS
C...  ...RECORD A NEW ADJACENT FIELD NUMBER.....................
  506 GO TO(517,517,517,517,517),NADJ
      NADJ=NADJ+1
      GO TO518
  517 NADJ=6
  518 IFL=2
      NADJ(NADJ)=IB
      GO TO 114
C        RESET   ADJCLASS  IFL=1
   ?? IFL=1
```

```
C         SECTION    2
C...   ...START COMPILING TEMPORARY STATISTICS.....................
  114 GO TO(510),IGRNUM
  113 SUMER=N
      NUMER=1
      SUMER2=N*N
      IGRNUM=1
      JSL=J
      GO TO 102
C...   ...CONTINUE COMPILING TEMPORARY STATISTICS.....................
  510 SUMER=SUMER+N
      NUMER=NUMER+1
      SUMER2=SUMER2+N*N
      GO TO 102
C...   ...IF GRADIENT IS GREATER THAN OR EQUAL TO THE THRESHOLD.....
C...   ...CHECK IF PREVIOUS POINT A WAS A FIELD .....................
  111 GO TO(511,514),IGRNUM
      GO TO 102
C...   ...YES PREVIOUS POINT WAS A FIELD  ...........................
  511 K8=0
      LOW=256
      LREAL=256
      GO TO(221,221,221,221,131),NADJ
      GO TO 223
  221 GO TO(222,222),NUMER
      GO TO 131
  222 LREAL=5
      GO TO 144
  223 DO 502  IW=6,NADJ
  515 L=MADJ(IW)
C...   ...COMPARE LOWEST ADJACENT FIELD NUMBER.......................
  504 IF(L-LOW)150,503,503
  150 K8=K8+1
      LOW=L
      LS(K8)=LOW
      L=LA(LOW)
      GO TO504
  503 IF(LOW.LT.LREAL)LREAL=LOW
      LOW=256
  502 CONTINUE
C...   ...UPDATE ADJACENT FIELD (TRANSLATION) TABLE WITH LOWEST .....
C...   ...ADJACENT FIELD.............................................
      DO 128  K9=1,K8
      K1=LS(K9)
  128 LA(K1)=LREAL
      GO TO 512
  131 ICD=ICD+1
  132 LREAL=ICD
C...   ...COMPARE MAXIMUM FIELD NUMBER TO 256.......................
      IF(ICD-256)144,144,144

      MLAS=J-1
      CALL TRANSF(ERR,K,MLAS,MDIN,MDOUT)
      GO TO 141
  144 CONTINUE
      LA(LREAL)=LREAL
  512 JEND=J-1
C...   ...CODE FIELD STRINGS IN THE DATA.............................
      DO 129 K9=JSL,JEND
  129 DEC(K9)=LREAL
      NADJ=4
      IFL=1
      IGRNUM=2
      NUM(LREAL,1)=NUM(LREAL,1)+NUMER
      SUM(LREAL,1)=SUM(LREAL,1)+SUMER
      SUM2(LREAL,1)=SUM2(LREAL,1)+SUMER2
  514 DEC(J)=IDIRX(X,Y)
  102 IFLG=ICD
C...   ...NO PREVIOUS POINT A WAS NOT A FIELD.......................
C...   ...A CLASS AT LINE END.......................................
      GO TO(511),IGRNUM
      ID=3
      ICD=4
      CALL MASMOV(NZ,LINE,LIN1)
      CALL MASMOV(NZ,DEC,DEC1)
      WRITE(MDIN,1010)(DEC1(I),I=1,KD)
  101 CONTINUE
      MLAS=J-1
```

```
C...  ...GO TO TRANSLATION SUBROUTINE.....................................
      CALL TRANS(IERR,K,MLAS,MDIN,MDOUT)
  141 WRITE(LP,1001)
      DO 130 I=6,ICD
      NUM=NUM(I,1)
      IF(NUM.EQ.0)GO TO777
      AVE=SUM(I,1)/NUM
      SD=(SUM2(I,1)/NUM(I,1)-AVE*AVE)**.5
C...  ...LIST STATISTICS OF PERMANENT ADJACENT FIELDS.....................
  130 WRITE(LP,1002)I,NUM(I,1),AVE,SD,SUM(I,1),SUM2(I,1)
      CALL CLSAPE
C        FORMATS
 2000 FORMAT(' THERE ARE',I5,'ELEMENTS IN CLASS',I5,10X,I5,'ADJ CLASS')
 2001 FORMAT(' DEC',3II4)
 1007 FORMAT('0',' MAIN PGM DEC'/(32I4))
 1015 FORMAT('0','IFLG=',I3,' GRAD DIR=',I3)
 1010 FORMAT(20(100A2))
 1000 FORMAT(6I5)
 1001 FORMAT('1',10X,'*  AREA  *  NUM OF PIXEL  *  AVERAGE  *  STANDARD
     1 DEV  *      SUM      *      SUMSQR      *')
 1002 FORMAT('0',10X,'*  ',I4,'  *  ',I12,'  *  ',F8.4,'  *  ',F13.4,'
     C* ',I11,' * ',I14,' *')
 1003 FORMAT(1X,(260A1))
 2006 FORMAT(' START COUNTING A CLASS AT POINT',I5,' AND LINE',I5)
 2009 FORMAT(' OH BOY OHBOY OHBOY OHBOY OH BOY',I5)
 2007 FORMAT(' NADJ=',I5,10X,'ADJ CLASS=I8=',I5)
 2008 FORMAT(' FINISH A CLASS',2I10)
  777 STOP
      END
C*********************************************************************
C
C        FUNCTION   FOR COMPUTATION OF DIRECTION OF GRADIENT VECTOR
      FUNCTION IDIRX(X,Y)
      IF(.NOT.(X.EQ.0.AND.Y.EQ.0))GO TO 5
      IDIRX=0
      RETURN
    5 IF(X.EQ.0)X=.001
      RAT=Y/X
      IF(.NOT.(RAT.GT..4142.AND.RAT.LT.2.4142))GO TO 1
      IDIRX=2
      RETURN
    1 IF(.NOT.(RAT.LT.-.4142.AND.RAT.GT.-2.4142))GO TO 2
      IDIRX=4
      RETURN
    2 RAT=ABS(RAT)
      IDIRX=3
      IF(RAT.LT.2.4142)GO TO 3
      RETURN
    3 IDIRX=1
      RETURN
      END
C*********************************************************************
C
C        TRANSLATION ROUTINE
      SUBROUTINE  TRANS(IERR,K,MLAS,MDIN,MDOUT)
C        IBG IS THE LOWEST CLASS NOT ALREADY PERMANENTLY ASSIGNED
      INTEGER*4 NUM,SUM,SUM2
      INTEGER*2 DEC1(1024),DEC,LA
      COMMON NUM(256,2),SUM(256,2),SUM2(256,2),IBG,ICD,II,LA(2048)
      COMMON DEC(1024),LC(256)
      LOGICAL*1  C(2048)
      EQUIVALENCE(C(1),DEC(1))
      LOGICAL*1 LC,A(512),LD(512)
      INTEGER*2  D(256)
      EQUIVALENCE (DEC1(1),LC(1))
      EQUIVALENCE (LA(1),A(1))
      EQUIVALENCE   (LD(1),D(1))
      D(1)=1
      D(2)=2
      D(3)=3
      D(4)=4
      D(5)=5
      REWIND MDIN
      ICR=5
      LP=6
```

```
      WRITE(LP,1006)ICD,II,MLAS
      NGRT=4
 1006 FORMAT('0','ICD=  ',I10,' LINE ',I5,' ELEMENT ',I5)
      WRITE(LP,1004)(LA(I),I=5,ICD)
 1004 FORMAT('0',' TABLE LA(I) BEFORE TRANSLATION'/('0',32I4))
      IOFFST=IBG-1
      DO 256 I=5,ICD
      NUM(I,2)=0
      SUM(I,2)=0
  256 SUM2(I,2)=0
      IFX=ICD-1
C...  ...REDUCE OVERALL ADJACENCY TABLE TO LOWEST ADJACENT FIELDS.......
      DO 250 I=6,IFX
      M=I
  301 L=LA(M)
      IF(L.EQ.M)GO TO 300
      M=LA(L)
      GO TO 301
  300 IF(L-NGRT)251,251,252
  251 MBG=D(LA(L))
      GO TO 240
  252 IBG=IBG+1
      NGRT=L
      MBG=IBG
C...  ...REDUCE TEMPORARY STATISTICS INTO.............................
C...  ...PERMANENT ADJACENT FIELD STATISTICS.........................
  240 NUM(MBG,2)=NUM(MBG,2)+NUM(I,1)
      SUM(MBG,2)=SUM(MBG,2)+SUM(I,1)
      SUM2(MBG,2)=SUM2(MBG,2)+SUM2(I,1)
      NUM(I,1)=0
      SUM(I,1)=0
      SUM2(I,1)=0
      D(I)=MBG
  250 CONTINUE
C*********************************************************************
C       IBG IS NOW THE NEW LAST NUMBER FOR CLASES OR NEW FICD)
C       LA IS NOW A VECTOR OF TRANSLATIONS FOR CLASS ADJACENCY
C       COMBINE OLD M
C       COMBINE OLD NUM INTO NEW NUM,(SUM, SUM2)
C*********************************************************************
      IEND=II-1
      DO 257 I=5,IBG
      NUM(I,1)=NUM(I,2)
      SUM(I,1)=SUM(I,2)
  257 SUM2(I,1)=SUM2(I,2)
      CALL MASMOV(512,LD,LA)
      DO 254 I=2,512,2
  254 LD(I/2)=LD(I)
      WRITE(LP,1005)(LD(I),I=5,ICD)
 1005 FORMAT('0','TABLE LD(I)'/('0',32I4))
      CALL MORTAB(1,ICD,LD,IER,1)
C
C
      ICD=IBG+1
      WRITE(LP,1011)KD
 1011 FORMAT('0','KD=  ',I3)
      KD=K-2
      KE=2*KD
      WRITE(LP,1009)
      DO 260 KI=1,IEND
C...  ...READ TEMPORARY FIELD NUMBERS FROM DISC.....................
      READ(MDIN,1010)(DEC1(I),I=1,KD)
      DO 259 M=2,KE,2
  259 LC(M/2)=LC(M)
C...  ...TRANSLATE TEMPORARY FIELD NUMBERS TO PERMANENT FIELDS.....
      CALL TRNTAB(0,KD,DEC1,IER,1)
C...  ...WRITE PERMANENT FIELDS ON TAPE..............................
  260  WRITE(MDOUT,1003)(LC(I),I=1,KD)
      M=MDIN
      MDIN=MDOUT
      MDOUT=M
 1008 FORMAT('0',32I4)
 1009 FORMAT(' ','TRANSLATED DEC1')
      M=2*MLAS
      DO 150 I=2,M,2
  150 LD(I/2)=C(2)
      CALL TRNTAB(0,MLAS,D,IER,1)
      DO 151 I=2,M,2
  151 LC(I)=LD(I/2)
      IF(ICD.EQ.256)IERR=1
 1003 FORMAT(120(100A1))
 1010 FORMAT(20(100A2))
 1019 FORMAT(' ',32I4)
      RETURN
      END
```

t-TEST COMPUTER PROGRAM

```
COMPILER OPTIONS - NAME=  MAIN,OPT=00,LINECNT=60,SIZE=0000K,
                   SOURCE,BCD,NOLIST,NODECK,LOAD,NOMAP,NOEDIT,NOID,NOXREF
            DOUBLE PRECISION DEGF,ANGLE,SINA,COSA,FACT1,FACT2,JFACT,KFACT,
           *ANGLEP,PI,TVAL,DVALUE,SIGLEV
            INTEGER F(2),C(2)
            DIMENSION FMT(20),   FMI(40),   FMO(40)
            INTEGER STCLAS,OUTPT,STCLA
            DATA ICR,LP,I,J/05,06,1,2/
            DOUBLE PRECISION  NUM(2),SUMX(2),SUMX2(2),AVE(2),      PVAL
            PI=3.14159265358979323846264338
     60     FORMAT(4I5,2F5.2)
     62     FORMAT(20A4)
     63     FORMAT('2')
     64     FORMAT('+',100X,F12.6,F5.1)
            READ(ICR,60)NFEAT,NCLASS,INPUT,STCLAS,SIGLEV,DVALUE
            READ(ICR,62)FMT,FMI,FMO
            DO 52 II=1,NFEAT
            STCLA=STCLAS
            WRITE(LP,63)
            I=1
            J=2
            READ(INPUT,FMT)(F(K),C(K),NUM(K),SUMX(K),SUMX2(K),AVE(K),K=1,2)
            DO 52 JJ=2,NCLASS
      C.....CALCULATE THE DEGREES OF FREEDOM AND X VALUE FOR THE
      C                  T-DISTRIBUTION .
            DEGF=NUM(I)+NUM(J)-2.0
            TVAL=(SUMX(I)/NUM(I)-SUMX(J)/NUM(J)-DVALUE)/((DSQRT(1.0/NUM(I)+1.0
           $/NUM(J)))*DSQRT((SUMX2(I)+SUMX2(J)-(SUMX(I)*SUMX(I))/NUM(I)-(SUMX(
           $J)*SUMX(J))/NUM(J))/DEGF))
            ID=DEGF
            LB=MOD(ID,2)
            IF(LB.EQ.1) GO TO 20
      C.....EVEN CALCULATION.
            IF(ID.GT.100) ID=100
            GO TO 24
      C.....ODD CALCULATION.
     20     IF(ID.GT.99) ID=99
     24     DEGF=ID
            ANGLE=DATAN(TVAL/(DSQRT(DEGF)))
            GO TO (42),ID
            SINA=DSIN(ANGLE)
            COSA=DCOS(ANGLE)
            ID=ID-2
            PVAL=1.0
            JFACT=1.0
            KFACT=1.0
            IF(ID.LT.2) GO TO 30
            DO 26 IFA=2,ID,2
            FA=IFA
            GO TO (25),LB
            JFACT=JFACT*(FA-1.0)
            GO TO 29
     25     JFACT=JFACT*(FA+1.0)
     29     KFACT=KFACT*FA
            ANGLEP=1.0
            DO 27 IRP=1,IFA
     27     ANGLEP=ANGLEP*COSA
            FACT1=JFACT
```

```
      FACT2=KFACT
C.....CALCULATE THE SIGNIFICANT LEVEL OF THIS SOLUTION.
      GO TO (32),LB
      PVAL=PVAL+((FACT1/FACT2)*ANGLEP)
      GO TO 26
 32   PVAL=PVAL+((FACT2/FACT1)*ANGLEP)
 26   CONTINUE
 30   PVAL=PVAL*SINA
      GO TO (34),LB
  33   GO TO 44
 34   PVAL=PVAL*((2.0/PI)*COSA)+((2.0*ANGLE)/PI)
      GO TO 44
 42   PVAL=2.0*ANGLE/PI
 44   IF(PVAL.GE.SIGLEV) GOTO 48
C.....SIGNIFICANT LEVEL TO SMALL SUM TOGETHER CLASSES AND RETRY.
      NUM(I)=NUM(I)+NUM(J)
      SUMX(I)=SUMX(I)+SUMX(J)
      SUMX2(I)=SUMX2(I)+SUMX2(J)
      WRITE(LP,FMI)F(I),C(I),C(J),AVE(I),PVAL
      WRITE(LP,64)TVAL,DEGF
 46   READ(INPUT,FMT,END=52)F(J),C(J),NUM(J),SUMX(J),SUMX2(J),AVE(J)
      GO TO 52
 48   WRITE(LP,FMO)F(I),C(I),STCLA,AVE(I),PVAL
      WRITE(LP,64)TVAL,DEGF
      STCLA=STCLA+1
      GO TO (49,50),I
 49   I=2
      J=1
      GO TO 46
 50   I=1
      J=2
      GO TO 46
 52   CONTINUE
      STOP
      END
```